

Wirelessly Powered Federated Edge Learning: Optimal Tradeoffs Between Convergence and Power Transfer

Qunsong Zeng, Yuqing Du, and Kaibin Huang

Abstract

Federated edge learning (FEEL) is a widely adopted framework for training an *artificial intelligence* (AI) model distributively at edge devices to leverage their data while preserving their data privacy. The execution of a power-hungry learning task at energy-constrained devices is a key challenge confronting the implementation of FEEL. To tackle the challenge, we propose the solution of powering devices using *wireless power transfer* (WPT). To derive guidelines on deploying the resultant *wirelessly powered FEEL* (WP-FEEL) system, this work aims at the derivation of the tradeoff between the model convergence and the settings of power sources in two scenarios: 1) the transmission power and density of power-beacons (dedicated charging stations) if they are deployed, or otherwise 2) the transmission power of a server (access-point). The development of the proposed analytical framework relates the accuracy of distributed stochastic gradient estimation to the WPT settings, the randomness in both communication and WPT links, and devices' computation capacities. Furthermore, the local-computation at devices (i.e., mini-batch size and processor clock frequency) is optimized to efficiently use the harvested energy for gradient estimation. The resultant learning-WPT tradeoffs reveal the simple scaling laws of the model-convergence rate with respect to the transferred energy as well as the devices' computational energy efficiencies. The results provide useful guidelines on WPT provisioning to provide a guarantee on learning performance. They are corroborated by experimental results using a real dataset.

I. INTRODUCTION

Recent years have seen a growing trend of deploying machine learning algorithms at the wireless network edge to distill *artificial intelligence* (AI) from the abundant data at edge devices (e.g., sensors and smart phones), giving rise to an area called *edge learning* [1], [2]. Among others, *federated edge learning* (FEEL) is perhaps the most widely adopted framework for its feature of preserving data privacy [3]–[5]. Specifically, instead of uploading data from devices, the framework involves a server distributing a learning task over devices based on distributed implementation of *stochastic gradient descent* (SGD). One challenge confronting

federated learning in practice is that executing a complex task (e.g., training of a large-scale *convolutional neural network* (CNN)) at edge devices drains their batteries. To tackle this challenge, we propose the solution of deploying *wireless power transfer* (WPT) to deliver to devices the energy they need for computation and communication. To understand the performance of the resultant *wirelessly powered FEEL* (WP-FEEL) system, this work aims at quantifying the optimal tradeoffs between model convergence and settings of power sources, which can be power-beacons (charging stations) or the server, when devices optimally allocate harvested energy for computation and communication to accelerate convergence. The derived tradeoffs, termed the optimal *learning-WPT tradeoffs*, yield useful insights into system design and deployment.

The current research on implementing FEEL in wireless networks can be separated into two main thrusts focusing on tackling two different challenges. One challenge is the communication bottleneck arising from the wireless uploading of high-dimensional model updates (either local models or local stochastic gradients) from many devices. Attempts to overcome the bottleneck have led to the design of a new class of communication techniques for efficient FEEL including over-the-air updates aggregation [5]–[7], resource management [8]–[10], adaptive uploading frequency control [4], device scheduling [11], and quantization [12]. The other challenge is to execute energy consuming tasks at edge devices as mentioned earlier. This issue has been addressed in a series of works on designing techniques for jointly managing computation and communication resources [13]–[16] under the criterion of minimizing the total devices’ energy consumption during the learning process. Addressing the same issue, we propose an alternative and direct approach of powering devices using WPT. Though there exist rich convergence analysis in the prior work, the tradeoffs between energy consumption of devices and convergence have not yet been crystallised. The derivation of the desired learning-WPT tradeoff is even more complex due to new issues arising from WPT especially the following two. First, the unreliabilities of both communication and WPT links jointly affect the number of active devices. Second, each device needs manage harvested energy for both communication and computation. Their coupling results in the channel dependence of local computation (i.e., mini-batch size and processor frequency) and hence learning performance.

There exists a rich literature on the application of microwave based WPT to power different types of wireless networks ranging from communication networks to sensor networks to those supporting mobile-edge computing (see recent surveys in [17], [18]). There exist three main topologies of wirelessly powered networks [19]: 1) the integration of WPT with downlink

transmission, called *simultaneous wireless information and power transfer* (SWIPT) (see e.g., [20]), 2) downlink WPT to power uplink transmission (see e.g., [21]), and 3) separated WPT served by power-beacons and radio access by base stations (see e.g., [22]). As the communication bottleneck of a FEEL system lies in the uplink, the last two topologies are relevant, both of which are considered in this paper. Despite building on the existing network topologies, WP-FEEL systems differ from their conventional wirelessly powered communication systems in several aspects. First, the performance of the former is measured using learning related metrics (i.e., convergence rate or test accuracy) and that of the latter is measured by communication related metrics such as throughput (see e.g., [21]), communication energy efficiency (see e.g., [23]), and rate-harvested-energy tradeoff (see e.g., [24]). Second, the devices in a WP-FEEL system are workers cooperating in training a global model while those in a communication system are subscribers competing for power transfer and the use of radio resources. Third, computing power consumption is either neglected or abstracted as a constant for conventional systems focusing on communication (see e.g., [5], [8], [13]). In contrast, such consumption is at least comparable with its communication counterpart in a WP-FEEL system performing a computation intensive task. Thus, an elaborate model of the former is adopted in this work so that the analysis can be of practical relevance.

The above distinctions between WP-FEEL systems and their conventional counterparts give rise to new challenges in designing and analyzing the former. To tackle the challenges, the main contribution of this work is the development of a novel analytical framework for quantifying the optimal learning-WPT tradeoff of a WP-FEEL system. As a by-product, a scheme for the optimal control of local computation at devices is designed. The framework is first developed for the scenario where dense power-beacons are deployed to provide reliable WPT without fading, referred to as the *beacon-WPT* [22]. The key components of the framework and relevant findings are described as follows.

- 1) **Distributed Gradient Estimation:** *Global and local gradient deviations* are respectively defined as the expected deviation of a local gradient estimate and the global estimate from the ground truth computed using the global/local datasets. In existing convergence analysis, they are usually studied under the following assumptions: 1) i.i.d. data distributions at devices, 2) uniform mini-batch sizes, and 3) a fixed number of active devices (see e.g., [25]–[29]). While the first assumption lacks generality, the last two do not hold for the WP-FEEL system featuring random harvested energy, the mentioned channel-dependent heterogeneous

computation capacities, and a random number of active devices. To address the issue, we define a generalized system of global and local gradient deviations by relaxing the assumptions. By analyzing these measures, the convergence rate is related to the distribution of the set of active devices as well as the derived probability of a *computation-outage event*, which occurs when a device fails to harvest sufficient energy to support both communication and computation and hence becomes inactive.

- 2) **Local-Computation Optimization:** Consider an active device and an arbitrary round. After reserving sufficient transmission energy, the remaining harvested energy is used for local computation. Under the energy constraint, the mini-batch size and processor's computing speed are jointly optimized to minimize the local gradient deviation. They are shown to both increase *sub-linearly* with the computation energy and be inversely proportional to the device's computation capacity. In addition, the optimal mini-batch size is also inversely proportional to the workload for local gradient computation.
- 3) **Optimal Learning-WPT Tradeoff:** The tradeoff is derived based on characterizing the effects of WPT on distributed gradient estimation and devices' computation-and-communication capacities. Define the *spatial energy density* for beacon-WPT as the total energy transferred from beacons to a randomly located device per round, denoted as λ_{energy} . The difference between the convergence rate and its limit in the ideal case of using the global dataset is found to be inversely proportional to a sub-linear function of spatial energy density, namely $O\left(\lambda_{\text{energy}}^{-\frac{1}{3}}\right)$. The result provides some guidelines on power-beacon deployment (i.e., power and density) to provide a guarantee on the learning performance. Moreover, the difference is shown to decay as a weighted sum of sub-linear functions of individual computation energy efficiencies (i.e., required energy for processing a data sample). Each weight depends on the usefulness of a local dataset and specifically is the local gradient deviation for a single sample. The result suggests the need of considering devices' computation energy efficiencies in WPT provisioning.

The framework is extended to the other scenario of *server-WPT*, where the server transfers power to devices over fading channels [21]. In particular, the scaling laws described above remain the same except that the spatial-energy density is replaced with the energy beamed by the server to each device in a specific round.

The remainder of the paper is organized as follows. Mathematical models are introduced in Section II. In Section III, distributed gradient estimation is analyzed to relate the convergence

rate to the distribution and computation capacities of active devices. The optimal learning-WPT tradeoff for beacon-WPT is derived in Section IV and extended to the scenario of server-WPT in Section V. Experimental results are presented in Section VI, followed by concluding remarks in Section VII.

II. MATHEMATICAL MODELS

We consider a single-cell WP-FEEL system in a circular cell with the radius denoted as R . A server equipped with an array of L antennas coordinates FEEL over K single-antenna edge devices, represented by the index set $\mathcal{K} = \{1, \dots, K\}$. Devices are assumed to have high mobility and their locations are uniformly distributed in the cell and i.i.d. over rounds. The devices are powered by either beacon-WPT or server-WPT as illustrated in Fig. 1. In each round with a fixed duration T , each device first computes a local gradient and then transmits it to the server. Then each round is divided in two phases: local computation and gradient uploading (see Fig. 1), which last T^{cmp} and T^{cmm} seconds, respectively. The operations of devices are synchronized, resulting in the following time constraints for edge devices:

$$0 < t_k^{\text{cmp}} \leq T^{\text{cmp}} \quad \text{and} \quad 0 < t_k^{\text{cmm}} \leq T^{\text{cmm}}, \quad \forall k \in \mathcal{K}, \quad (1)$$

where t_k^{cmp} and t_k^{cmm} are the computation and transmission time at device k in one round, respectively. Let E_k denote the amount of energy harvested by device k ; its computation and communication energy consumptions are represented by E_k^{cmp} and E_k^{cmm} , respectively. The harvested energy is fixed for beacon-WPT and varies over rounds for server-WPT as elaborated in the sequel. They satisfy the following energy constraint:¹

$$E_k^{\text{cmp}} + E_k^{\text{cmm}} \leq E_k, \quad \forall k \in \mathcal{K}. \quad (2)$$

The detailed system operations and relevant models are described as follows.

A. Two WPT Models

1) *Beacon-WPT*: Consider the WP-FEEL system powered by beacon-WPT in Fig. 1(a). Given their low cost and complexity, dense power-beacons are deployed to power devices over short-range WPT links without fading. The beacons are modelled as a homogeneous *Poisson point*

¹To be precise, the idling circuit energy consumption, denoted as a constant ζ , exists even when there is no computation and transmission. In this case, the energy constraint is $E_k^{\text{cmp}} + E_k^{\text{cmm}} + \zeta \leq E_k$. We omit the constant ζ as it is negligible compared with E_k^{cmp} and E_k^{cmm} .

process (PPP), denoted as $\Psi = \{\mathbf{s}\}$ with density λ_{pb} , where $\mathbf{s} \in \mathbb{R}^2$ represent the coordinate of a single beacon. Each device is equipped with an energy harvester comprising a rectifying antenna and a battery [19]. Moreover, WPT is over a dedicated frequency outside the communication band. These allow the device to continuously harvest energy throughout the learning process [see Fig. 1(a)]. Let the coordinates of device k in the i -th round be denoted by $\mathbf{r}_k^{(i)}$ and thus the communication range $r_k^{(i)} = |\mathbf{r}_k^{(i)}|$. Adopting a short-range propagation model [30], the instantaneous power received at the device k in round i is given as

$$P_k^{(i)} = \rho \bar{P} \sum_{\mathbf{s} \in \Psi} \left(\max\{|\mathbf{r}_k^{(i)} - \mathbf{s}|, \nu\} \right)^{-\beta}, \quad \forall k \in \mathcal{K}, \quad (3)$$

where $\nu \geq 1$ is a given constant avoiding singularity, $\beta > 2$ is the path-loss exponent, \bar{P} is the transmission power of power-beacons, and ρ represents the product of energy-conversion efficiency and energy-beamforming gain. As the power-beacons are dense and homogeneously distributed in the cell, the amount of harvested energy at each device in one round can be approximated as [22]

$$E_k^{(i)} \approx \bar{E} = \frac{\pi \beta \rho \bar{P} \lambda_{\text{pb}} T}{(\beta - 2) \nu^{\beta-2}}, \quad \forall k \in \mathcal{K}. \quad (4)$$

Definition 1. (*Spatial-Energy Density*) The spatial-energy density is defined as $\lambda_{\text{energy}} \triangleq \bar{P} \lambda_{\text{pb}} T$, which is proportional to the beacon density and transmission power. It can be interpreted as the amount of energy delivered by the power-beacon network to an arbitrarily located device in a single round.

2) *Server-WPT*: In the absence of power-beacons, devices can be also powered by the server over long-range WPT links with fading as illustrated in Fig. 1(b). The server is assumed to be half-duplex and thus can perform WPT only during the local-computation phase in each round when its array is not used for communication [see Fig. 1(b)]. Let the isotropic complex Gaussian vector $\tilde{\mathbf{h}}_k^{(i)} \in \mathbb{C}^{L \times 1}$ represent the Rayleigh fading channel of the WPT link from the server to device k . Moreover, let $\mathbf{u}_k^{(i)} \in \mathbb{C}^{L \times 1}$ with $(\mathbf{u}_k^{(i)})^H \mathbf{u}_k^{(i)} = 1$ denote the energy-beamforming vector, and $\tilde{P}_k^{(i)}$ the transfer power allocated to device k . With energy beamforming, the amount of harvested energy by device k in each round is given as

$$E_k^{(i)} = \rho (r_k^{(i)})^{-\alpha} \|\tilde{\mathbf{h}}_k^{(i)}\|^2 \tilde{P}_k^{(i)} T^{\text{cmp}}, \quad \forall k \in \mathcal{K}. \quad (5)$$

Last, the WPT channels are assumed to be i.i.d. over rounds and furthermore independent of the uplink channels since they are in different frequency bands.

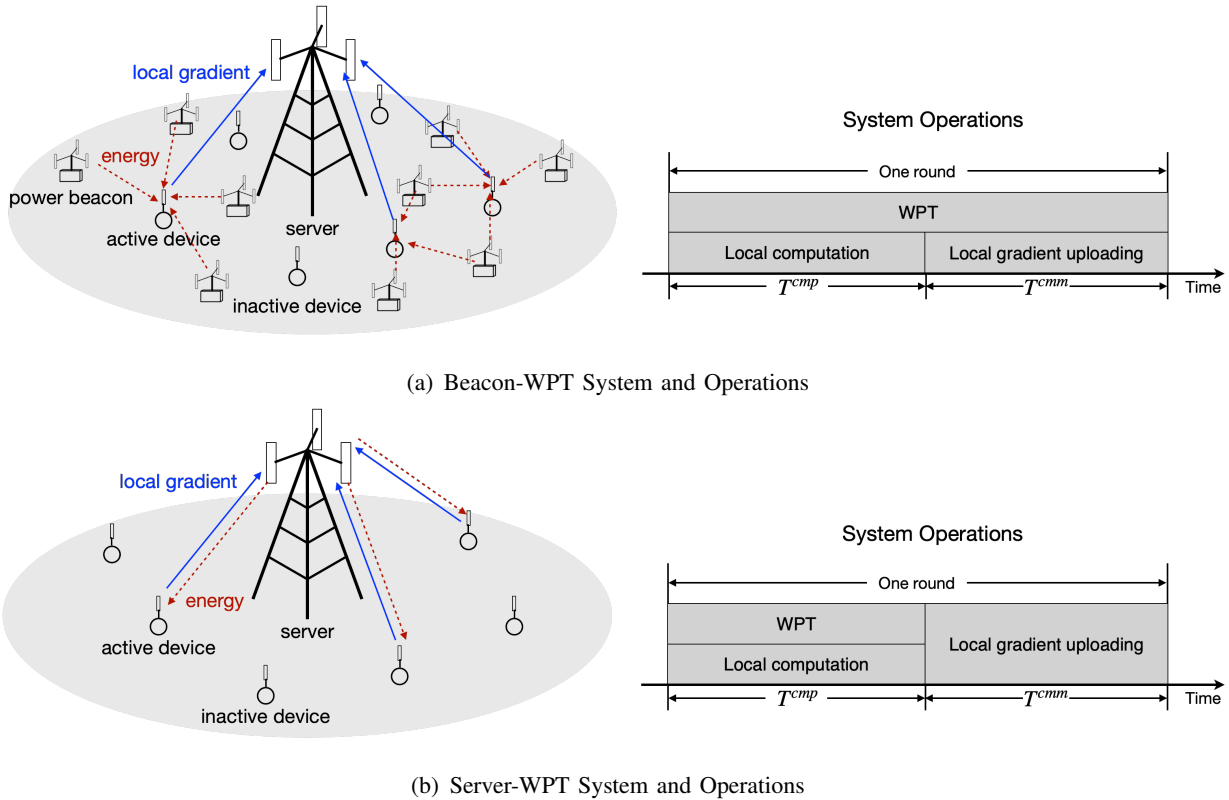


Figure 1. WP-FEEL systems and operations: (a) beacon-WPT and (b) server-WPT.

B. Federated Learning Model

A standard federated learning framework is considered as follows (see e.g., [31]). A global model, represented by the parametric vector $\mathbf{w} \in \mathbb{R}^q$ with q denoting the model size, is trained collaboratively across the edge devices by leveraging local labelled datasets. For device k , let $\mathcal{D}_k = \{(\mathbf{x}_j, y_j)\}$ denote the local dataset where \mathbf{x}_j and y_j represent the raw data and label of the j -th sample. The *local loss function* is defined as

$$F_k(\mathbf{w}) = \frac{1}{|\mathcal{D}_k|} \sum_{(\mathbf{x}_j, y_j) \in \mathcal{D}_k} \ell(\mathbf{w}; (\mathbf{x}_j, y_j)), \quad (6)$$

where $\ell(\mathbf{w}; (\mathbf{x}_j, y_j))$ is the sample-wise loss function quantifying the prediction error of the model \mathbf{w} on the training sample \mathbf{x}_j with reference to its true label y_j . For convenience, we denote $\ell(\mathbf{w}; (\mathbf{x}_j, y_j))$ as $\ell_j(\mathbf{w})$ and assume uniform sizes for local datasets: $|\mathcal{D}_k| = D, \forall k \in \mathcal{K}$. Then the *global loss function* on all the distributed datasets can be written as

$$F(\mathbf{w}) = \frac{\sum_{k=1}^K \sum_{j \in \mathcal{D}_k} \ell_j(\mathbf{w})}{\sum_{k=1}^K |\mathcal{D}_k|} = \frac{1}{K} \sum_{k=1}^K F_k(\mathbf{w}). \quad (7)$$

Its gradient $\nabla F(\mathbf{w}^{(i)})$ is referred to as the *ground-truth gradient*. The learning process is to minimize the global loss function $F(\mathbf{w})$. To this end, each round aims at estimating $\nabla F(\mathbf{w}^{(i)})$ distributively to facilitate SGD.

We adopt the existing gradient-averaging implementation of FEEL with the key operations illustrated in Fig. 2 and described as follows (see e.g., [9]). In each round, say the i -th round, the server broadcasts the current model $\mathbf{w}^{(i)}$ to all edge devices. Due to channel fading, only a subset of devices, denoted as a subset $\mathcal{M}^{(i)} \subseteq \mathcal{K}$ with size $M^{(i)} = |\mathcal{M}^{(i)}|$, can participate in learning in this specific round. Each device in $\mathcal{M}^{(i)}$ computes a local estimate of the gradient of its local loss function by randomly sampling its local dataset \mathcal{D}_k . We denote the sampled mini-batch local dataset as $\mathcal{B}_k^{(i)}$ whose size is denoted by $b_k^{(i)} = |\mathcal{B}_k^{(i)}|$. The local gradient at device k in the i -th round is estimated using the mini-batch as

$$\mathbf{g}_k^{(i)} = \frac{1}{b_k^{(i)}} \sum_{(\mathbf{x}_j, y_j) \in \mathcal{B}_k^{(i)}} \nabla \ell_j(\mathbf{w}^{(i)}). \quad (8)$$

Upon completion, the local gradient estimates are sent by active devices to the server for aggregation. Upon receiving them, the global gradient is calculated as

$$\mathbf{g}^{(i)} = \begin{cases} \frac{1}{M^{(i)}} \sum_{k \in \mathcal{M}^{(i)}} \mathbf{g}_k^{(i)}, & M^{(i)} > 0 \\ \mathbf{0}, & M^{(i)} = 0 \end{cases}. \quad (9)$$

Subsequently, the global model is then updated using SGD as

$$\mathbf{w}^{(i+1)} = \mathbf{w}^{(i)} - \eta \mathbf{g}^{(i)}, \quad (10)$$

where η is the given learning rate. The process iterates until the model converges. In the process, the accuracy of distributed gradient estimation can be measured using the following metrics.

Definition 2. (*Local and Global Gradient Deviations*). In the i -th round, the local gradient deviation at device k , denoted as $G_{\text{lo},k}^{(i)}$, refers to the mean-square error between the local gradient estimate and its ground-truth:

$$G_{\text{lo},k}^{(i)} = \mathbb{E} \left[\|\mathbf{g}_k^{(i)} - \nabla F_k(\mathbf{w}^{(i)})\|^2 \right]. \quad (11)$$

The global gradient deviation refers to the expected deviation between the aggregated local gradient estimates at the server and the ground truth:

$$G_{\text{gl}}^{(i)} = \mathbb{E}_{\mathcal{M}^{(i)}} \left\{ \mathbb{E} \left[\|\mathbf{g}^{(i)} - \nabla F(\mathbf{w}^{(i)})\|^2 \right] \right\}, \quad (12)$$

where the outer expectation is taken over rounds and the distributions of $M^{(i)}$ and $b_k^{(i)}$.

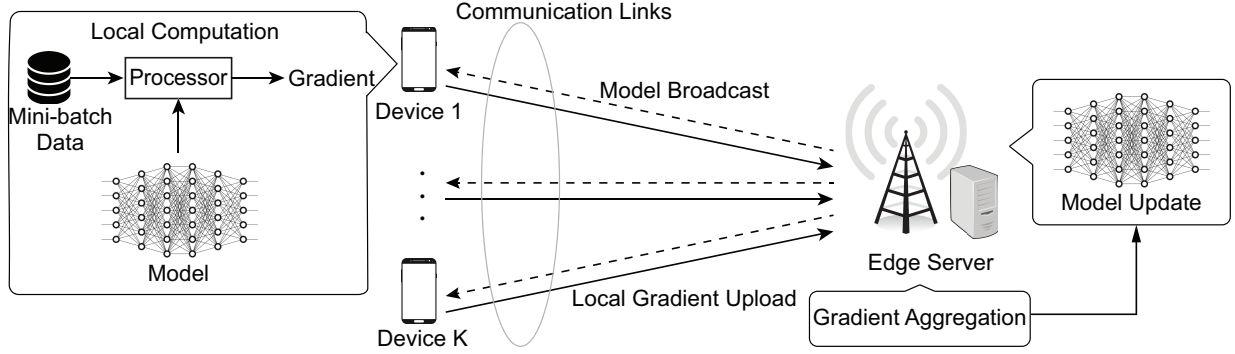


Figure 2. FEEL Operations.

C. Local-Computation Model

The computation-energy consumption depends on two variables: 1) the mini-batch size and 2) the processor's clock frequency. Adopting a standard model in computer engineering [32], we define the per-sample workload W for local-gradient estimation as the number of *floating point operations* (FLOPs) needed for processing each data sample. This gives the workload at device k in the i -th round as $W_{k,\text{total}}^{(i)} = b_k^{(i)} \times W$. Let $f_{\text{clk},k}^{(i)}$ [in cycle/s] represent the clock frequency of the processor (e.g., CPU or GPU) at device k in round i . As a result, the computing speed of the processor, measured in FLOPs per second, can be defined as $f_k^{(i)} = f_{\text{clk},k}^{(i)} \times N_k^{\text{FLOP}}$ with N_k^{FLOP} denoting the number of FLOPs it can process per cycle. Given the workload and computing speed, the local computation time at device k , denoted as $t_k^{\text{cmp}(i)}$, is given by

$$t_k^{\text{cmp}(i)} = \frac{b_k^{(i)}W}{f_k^{(i)}}, \quad \forall k \in \mathcal{K}. \quad (13)$$

For a CMOS circuit, the power consumption of a processor can be modelled as a function of clock frequency: $P = \Psi f_{\text{clk}}^3$, where Ψ [in Watt/(cycle/s)³] is a constant depending on the chip architecture [33]. Based on this model, the power consumption of the processor at device k can be written as

$$P_k^{\text{cmp}(i)} = \Psi_k (f_{\text{clk},k}^{(i)})^3 = C_k (f_k^{(i)})^3, \quad \forall k \in \mathcal{K}, \quad (14)$$

where the coefficient $C_k = \Psi_k / (N_k^{\text{FLOP}})^3$ characterizes the computation property of the processor. In particular, a smaller value indicates that the processor is capable to compute more workload given energy consumption per unit time, or consume less energy given the workload per unit time. Given (13) and (14), the resultant energy consumption at device k is given as

$$E_k^{\text{cmp}(i)} = P_k^{\text{cmp}(i)} \times t_k^{\text{cmp}(i)} = b_k^{(i)} C_k W (f_k^{(i)})^2, \quad \forall k \in \mathcal{K}. \quad (15)$$

D. Transmission Model

Without loss of generality, consider uploading by device k in the i -th round. Each gradient coefficient is compressed into Q bits such that the effect of quantization on the learning performance is negligible. Then the overhead of transmitting a q -dimensional vector is $q \times Q$ bits. The uplink bandwidth is equally divided into K narrow sub-bands of B and allocated to the devices for orthogonal transmission. Let the complex Gaussian vector $\mathbf{h}_k^{(i)}$ comprising i.i.d. $\mathcal{CN}(0, 1)$ coefficients represent the Rayleigh fading channel of the considered devices. Channels of different devices are assumed independent of each other. Given receive beamforming at the server, the transmission rate for device k in round i can be written as

$$S_k^{(i)} = B \log_2 \left(1 + \frac{\|\mathbf{h}_k^{(i)}\|^2 P_k^{\text{cmm}(i)}}{(r_k^{(i)})^\alpha B N_0} \right), \quad \forall k \in \mathcal{K}. \quad (16)$$

where $P_k^{\text{cmm}(i)}$ represents the transmission power, N_0 the power spectrum density of the additive white Gaussian noise, $r_k^{(i)}$ the propagation distance, and α the path-loss exponent. The transmission rate is required to support uploading of $q \times Q$ bits in a single round. This places the following constraint on the transmission power:

$$P_k^{\text{cmm}(i)} = \frac{(r_k^{(i)})^\alpha B N_0}{\|\mathbf{h}_k^{(i)}\|^2} \left(2^{\frac{qQ}{B t_k^{\text{cmm}(i)}}} - 1 \right), \quad \forall k \in \mathcal{K}. \quad (17)$$

The resultant transmission-energy consumption is

$$E_k^{\text{cmm}(i)} = P_k^{\text{cmm}(i)} \times t_k^{\text{cmm}(i)} = \frac{(r_k^{(i)})^\alpha}{\|\mathbf{h}_k^{(i)}\|^2} \varphi(t_k^{\text{cmm}(i)}), \quad \forall k \in \mathcal{K}, \quad (18)$$

where the function $\varphi(t) \triangleq B N_0 t \left(2^{\frac{qQ}{Bt}} - 1 \right)$.

III. CONVERGENCE AND DISTRIBUTED GRADIENT ESTIMATION

Consider the WP-FEEL system with beacon-WPT. In this section, we aim at analyzing the relation between convergence and several key system variables influencing the accuracy of distributed gradient estimation, including the mini-batch sizes of devices, number of active devices, and computation-outage probability. Such results are useful for deriving the learning-WPT tradeoff in the next section. As direct analysis is difficult, a tractable approach is adopted using global and local gradient deviations as intermediate variables.

A. Convergence and Global Gradient Deviation

To quantify the relation, we follow the literature to make several standard assumptions on the loss function and local estimated gradients as follows (see e.g., [4], [26]–[28], [34]–[37]).

Assumption 1. (*Smoothness*). The loss function $F : \mathbb{R}^q \rightarrow \mathbb{R}$ is μ -smooth. Specifically, for all $(\mathbf{u}, \mathbf{v}) \in \mathbb{R}^q \times \mathbb{R}^q$,

$$F(\mathbf{u}) \leq F(\mathbf{v}) + \langle \nabla F(\mathbf{v}), \mathbf{u} - \mathbf{v} \rangle + \frac{\mu}{2} \|\mathbf{u} - \mathbf{v}\|^2, \quad (19)$$

where ∇ is the differential operator and $\langle \cdot, \cdot \rangle$ represents the inner product.

While i.i.d. data distributions over devices are commonly assumed in the literature for simplicity (see e.g., [25]), we consider the general and more practical case of *non-i.i.d.* data distribution as in [35]. For the case of i.i.d. distributions, local gradients are unbiased with respect to the global full-batch gradient: $\mathbb{E}[\mathbf{g}_k] = \nabla F(\mathbf{w}), \forall k \in \mathcal{K}$, where the expectation is taken over the data distribution at device k . On the other hand, for the current case of non-i.i.d. distributions, we make the following assumption on local gradient estimates [35].

Assumption 2. (*Local Gradients Estimation*). The stochastic gradient estimates $\{\mathbf{g}_k\}$ defined in (8) are unbiased estimates of its local gradients $\{\nabla F_k(\mathbf{w})\}$ defined in (6) and computed using full local datasets, and independent of each other:

$$\mathbb{E}[\mathbf{g}_k] = \nabla F_k(\mathbf{w}), \quad \forall k \in \mathcal{K}, \quad (20)$$

where the expectation is taken over local data distribution \mathcal{D}_k .

It should be reiterated that local gradients are not equal to the global gradient and their relation is specified in (7). Our analysis does not require the convexity assumption for the loss function and only requires it to be lower bounded as formally stated below, which is the minimal assumption needed for ensuring convergence to a stationary point [36].

Assumption 3. (*Bounded Loss Function*). For any parameter vector \mathbf{w} , the loss function $F(\mathbf{w})$ is lower bounded by a given scalar F_* .

The last assumption given below is also standard in the literature (see e.g., [26]–[28]).

Assumption 4. (*Bounded Gradient Norm*). The expected squared norm of stochastic gradients is uniformly bounded by a constant Φ , that is, $\mathbb{E} \left[\|\mathbf{g}_k^{(i)}\|^2 \right] \leq \Phi, \forall k \in \mathcal{K}$ and $\forall i$.

We adopt a widely metric for measuring the convergence rate of FEEL with a non-convex loss function, namely the *expected average gradient norm* (over rounds) [29], [34], [37]. Based on the above assumptions, we prove that expected average gradient norm can be bounded by the average global gradient deviation as shown in the following proposition, thereby relating convergence to gradient estimation.

Proposition 1. Given the learning rate satisfying $0 < \eta \leq \frac{1}{\mu}$, the expected convergence rate of the FEEL algorithm can be upper-bounded by the average global gradient deviation as follows

$$\mathbb{E} \left[\frac{1}{N} \sum_{i=0}^{N-1} \|\nabla F(\mathbf{w}^{(i)})\|^2 \right] \leq \frac{2 [F(\mathbf{w}^{(0)}) - F_*]}{\eta N} + \frac{1}{N} \sum_{i=0}^{N-1} G_{\text{gl}}^{(i)}. \quad (21)$$

where $G_{\text{gl}}^{(i)}$ is defined in (12).

Proof: See Appendix A. □

B. Computation-Outage Probability

The computation-outage probability that affects the global gradient deviation is derived as follows. Without loss of generality, consider device k .

Definition 3. (*Computation-Outage Event*). The event occurs at device k in the i -th round when its harvested energy \bar{E} is no larger than the required transmission energy $E_k^{\text{cmm}}(r_k^{(i)}, \mathbf{h}_k^{(i)})$ given the propagation distance $r_k^{(i)}$ and fading channel $\mathbf{h}_k^{(i)}$. As a result, there is zero energy for computation and device k is inactive in round i : $k \notin \mathcal{M}^{(i)}$.

It is well known that the gain of the Rayleigh fading channel, $\|\mathbf{h}_k^{(i)}\|^2$, follows the χ^2 -distribution with the following *probability density function* (PDF):

$$f_{\|\mathbf{h}_k^{(i)}\|^2}(h) = \frac{h^{L-1} e^{-h}}{\Gamma(L)}, \quad h \geq 0, \quad (22)$$

where $\Gamma(\cdot)$ is the Gamma function. On the other hand, since each device is uniformly distributed in the cell, the transmission distance of device k has the following PDF:

$$f_{r_k^{(i)}}(r) = \frac{2r}{R^2}, \quad 0 \leq r \leq R. \quad (23)$$

Next, since transmission energy is a monotone decreasing function of the transmission duration, to minimize energy consumption requires the use of the maximum transmission duration: $t_k^{\text{cmm}(i)} = T^{\text{cmm}}$. Then the required transmission energy in round i is $E_k^{\text{cmm}}(r_k^{(i)}, \mathbf{h}_k^{(i)}) = \frac{(r_k^{(i)})^\alpha}{\|\mathbf{h}_k^{(i)}\|^2} \varphi(T^{\text{cmm}})$. Using the above results, the computation-outage probability is derived as follows.

Lemma 1. (*Computation-Outage Probability*). The probability is identical for all devices and all round and given as

$$P_{\text{out}} = \frac{\gamma(L, \xi) - \xi^{-\frac{2}{\alpha}} \gamma(L + \frac{2}{\alpha}, \xi)}{\Gamma(L)}, \quad (24)$$

where $\gamma(\cdot, \cdot)$ is the lower incomplete Gamma function, and the parameter ξ is defined as

$$\xi \triangleq \frac{\varphi(T^{\text{cmm}})}{R^{-\alpha} \bar{E}} = \frac{(\beta - 2) \nu^{\beta-2} R^\alpha \varphi(T^{\text{cmm}})}{\pi \beta \rho \bar{P} \lambda_{\text{pb}} T}. \quad (25)$$

Proof: See Appendix C. □

The parameter ξ defined in (25) is a key parameter influencing P_{out} . The asymptotic scalings of P_{out} with respect to ξ are characterized in the following corollary of Lemma 1.

Corollary 1. The computation-outage probability $P_{\text{out}}(\xi)$ is a monotone increasing function of the parameter ξ . Asymptotically, $P_{\text{out}}(\xi)$ scales with respect to ξ as follows:

$$\lim_{\xi \rightarrow 0} \frac{P_{\text{out}}(\xi)}{\xi^L} = \frac{2}{(\alpha L + 2) \Gamma(L + 1)} \quad \text{and} \quad \lim_{\xi \rightarrow \infty} \frac{1 - P_{\text{out}}(\xi)}{\xi^{-\frac{2}{\alpha}}} = \frac{\Gamma(L + \frac{2}{\alpha})}{\Gamma(L)}. \quad (26)$$

Based on the definition of ξ in (25), the above scaling laws suggest that the computation-outage probability can be reduced by 1) enhancing the harvested energy \bar{E} via increasing the density and transmission power of power-beacons or 2) decreasing the cell size.

Remark 1. (*Active and Idle Rounds*). A round is idle with learning paused when all devices are in outage (i.e., $M = 0$). The probability of idling round is $\Pr(M = 0) = P_{\text{out}}^K$ and that of active round is $\Pr(M > 0) = 1 - P_{\text{out}}^K$.

C. Effects of System Variables on Convergence

Given the result in Proposition 1, characterizing the effects requires only the analysis of the relation between the global gradient deviation and the system parameters. To this end, consider an arbitrary round and the superscripts i of variables, which specify the round index, are omitted in the remainder of the sub-section to simplify notation. An arbitrary active device, say device k , randomly draws a mini-batch of b_k samples with the index set $\mathcal{B}_k = \{j_1, \dots, j_{b_k}\}$. Then the local gradient estimate can be written as $\mathbf{g}_k = \frac{1}{b_k} \sum_{j \in \mathcal{B}_k} \nabla \ell_j(\mathbf{w})$. Its distribution is specified in the following lemma.

Lemma 2. (*Distribution of Local Gradient Estimate* [38]). At active device k , the first two moments of the local gradient estimate are given as $\mathbb{E}[\mathbf{g}_k] = \nabla F_k(\mathbf{w})$ and $\text{Var}[\mathbf{g}_k] = \frac{\Omega_k}{b_k}$ with Ω_k being a constant defined as $\Omega_k \triangleq \frac{1}{D} \sum_{j \in \mathcal{D}_k} \nabla \ell_j(\mathbf{w}) \nabla \ell_j(\mathbf{w})^\top - \nabla F_k(\mathbf{w}) \nabla F_k(\mathbf{w})^\top$.

It follows that the local gradient deviation at device k can be written as $G_{\text{lo},k} = \frac{\sigma_k^2}{b_k}$ with its single-sample variance $\sigma_k^2 \triangleq \text{tr}(\Omega_k)$. Based on Assumptions 2 and 3 and Lemma 2, we obtain the following useful result.

Lemma 3. The global gradient deviation in an arbitrary round can be bounded as

$$G_{\text{gl}} \leq \frac{2}{K^2} \mathbb{E} \left[\sum_{k \in \mathcal{M}} \frac{\sigma_k^2}{b_k} \right] + 2 \left\{ (1 - P_{\text{out}}^K) \left(\mathbb{E} \left[\frac{1}{M} \mid M > 0 \right] - \frac{1}{K} \right) + P_{\text{out}}^2 \right\} \Phi, \quad (27)$$

where P_{out} is given in (24).

Proof: See Appendix B. □

Combining Proposition 1 and Lemma 3 gives the main result of this sub-section.

Proposition 2. Given the learning rate satisfying $0 < \eta \leq \frac{1}{\mu}$, the expected convergence rate of the FEEL algorithm satisfies

$$\begin{aligned} \mathbb{E} \left[\frac{1}{N} \sum_{i=0}^{N-1} \|\nabla F(\mathbf{w}^{(i)})\|^2 \right] &\leq \frac{2 [F(\mathbf{w}^{(0)}) - F_*]}{\eta N} + \frac{2}{K^2} \mathbb{E} \left[\sum_{k \in \mathcal{M}} \frac{\sigma_k^2}{b_k} \right] \\ &+ 2 \left\{ (1 - P_{\text{out}}^K) \left(\mathbb{E} \left[\frac{1}{M} \mid M > 0 \right] - \frac{1}{K} \right) + P_{\text{out}}^2 \right\} \Phi. \end{aligned} \quad (28)$$

The above result relates convergence to several key system parameters, including the mini-batch sizes, number of active devices and its distribution, and computation-outage probability. In addition, one can observe that the upper bound in Proposition 2 is identical for all rounds and thus simplify the subsequent analysis.

IV. OPTIMAL LEARNING-WPT TRADEOFF FOR BEACON-WPT

In this section, we first give the optimized local computation policy, which determines how many samples the active devices can process in this round. Then, the global gradient deviation is derived by exploring the two factors that affect the global gradient deviation, respectively. The learning-energy tradeoff for beacon-WPT is characterized by the relation between convergence rate and spatial-energy density from the power-beacon network.

A. Local Computation Optimization

The local-computation variables at each device can be optimized to maximize the accuracy of local gradient estimation. On other hand, increasing the local batch size for model training reduces the local gradient deviation, but it increases local energy consumption according to (15).

Moreover, under the time constraint, processing more samples requires boosting the computing speed, which also contributes to the energy growth. Thus it is useful to control the two variables, sampled batch size and computing speed, under the criterion of minimum local gradient deviation. Considering device k without loss of generality, since the local gradient deviation, $G_{10,k}$, given in (11) is inversely proportional to the sampled batch size, b_k , the optimization problem can be formulated as

$$\begin{aligned}
 & \max_{\{b_k, f_k\}} b_k \\
 \text{(P1)} \quad & \text{s.t.} \quad 0 < b_k C_k W f_k^2 \leq E_k^{\text{cmp}}, \\
 & \quad \quad 0 < \frac{b_k W}{f_k} \leq T^{\text{cmp}}.
 \end{aligned}$$

For tractability, the batch size b_k is relaxed to be continuous. This is reasonable as the batch size for model training is usually large (e.g., thousands of images). With the relaxation, the optimal policy is derived in closed-form as shown below.

Lemma 4. (*Optimal Local-Computation Policy*). For optimal local gradient estimation at each active device, the optimal sampled batch size and the computing speed should be set as follows:

$$b_k^* = \frac{1}{W} \left(\frac{E_k^{\text{cmp}} (T^{\text{cmp}})^2}{C_k} \right)^{\frac{1}{3}} \quad \text{and} \quad f_k^* = \left(\frac{E_k^{\text{cmp}}}{C_k T^{\text{cmp}}} \right)^{\frac{1}{3}}, \quad \forall k \in \mathcal{M}. \quad (29)$$

The proof involves straightforward application of the *Karush–Kuhn–Tucker* (KKT) conditions and is omitted for brevity.

Given the optimal policy, the expectation of the resultant local gradient estimate at an active device is derived as follows. First, the expectation can be expressed in terms of the computation energy budget $\{E_k^{\text{cmp}}\}$ as

$$\mathbb{E} [G_{10,k}^* | k \in \mathcal{M}] = \frac{W}{(T^{\text{cmp}})^{\frac{2}{3}}} \mathbb{E}_{E_k^{\text{cmp}}} \left[\frac{\sigma_k^2 C_k^{\frac{1}{3}}}{(E_k^{\text{cmp}})^{\frac{1}{3}}} \middle| k \in \mathcal{M} \right]. \quad (30)$$

Since the transferred energy is equal to the sum of computation and transmission energy, we can write $\{E_k^{\text{cmp}}\}$ as the function of propagation distance and channel state as $E_k^{\text{cmp}}(r_k, \mathbf{h}_k) = \bar{E} - \frac{r_k^\alpha}{\|\mathbf{h}_k\|^2} \varphi(T^{\text{cmm}})$. It follows from (30) that

$$\Pr(k \in \mathcal{M}) \mathbb{E} [G_{10,k}^* | k \in \mathcal{M}] = \frac{W}{(T^{\text{cmp}})^{\frac{2}{3}}} \iint_{\Theta} \frac{\sigma_k^2 C_k^{\frac{1}{3}}}{(\bar{E} - E_k^{\text{cmm}}(r, h))^{\frac{1}{3}}} \frac{h^{L-1} e^{-h}}{\Gamma(L)} \frac{2r}{R^2} dr dh, \quad (31)$$

where the integral domain is defined as $\Theta = \{(r, h) \in \mathbb{R}^2 : \bar{E} > E_k^{\text{cmm}}(r, h); h \geq 0; 0 \leq r \leq R\}$.

Based on (31), we obtain the following result.

Lemma 5. (*Optimal Local Gradient Deviation*). Given optimal local computation in Lemma 4, the expectation of the local gradient deviation at each active device can be bounded as

$$\mathbb{E} [G_{10,k}^* | k \in \mathcal{M}] \leq \frac{2W\sigma_k^2 C_k^{\frac{1}{3}} B(\frac{2}{3}, \frac{2}{\alpha})}{\alpha(T^{\text{cmp}})^{\frac{2}{3}} \bar{E}^{\frac{1}{3}}}, \quad (32)$$

where $B(\cdot, \cdot)$ is the Beta function, and \bar{E} is the harvested energy at one device given in (4).

Proof: See Appendix D. □

B. Optimal Learning-WPT Tradeoff

So far we have analyzed two factors, local gradient deviation and computation-outage probability, which affect the global gradient deviation. To derive the desired learning-energy tradeoff with optimal local computation, we need to quantify the last factor, $\mathbb{E} \left[\frac{1}{M} \middle| M > 0 \right]$, with M being the number of active devices (see Proposition 3). This factor represents the fact that more active devices help improve the accuracy of global gradient estimation. To analyze the factor, whether each device participates in a round can be represented by a Bernoulli random variable with the parameter $(1 - P_{\text{out}})$, namely $\mathbb{I}_{k \in \mathcal{M}} \sim \text{Ber}(1 - P_{\text{out}})$, $\forall k \in \mathcal{K}$, where $\mathbb{I}_{k \in \mathcal{M}}$ denotes the indicator whose value is 1 if $k \in \mathcal{M}$, or 0 otherwise. It follows that $M \sim \text{Binom}(K, 1 - P_{\text{out}})$, which follows the Binomial distribution. The truncated version of the probability mass function with $M > 0$ is given as

$$\Pr(M = m) = \frac{1}{1 - P_{\text{out}}^K} \binom{K}{m} (1 - P_{\text{out}})^m P_{\text{out}}^{K-m}, \quad m = 1, \dots, K. \quad (33)$$

Using the distribution and a result from [39], the desired factor can be obtained as shown in the following lemma.

Lemma 6. (*Expected Reciprocal* [39]). The expected reciprocal of the number of active devices, M , can be written in terms of the computation-outage probability as follows:

$$\mathbb{E} \left[\frac{1}{M} \middle| M > 0 \right] = \frac{1}{1 - P_{\text{out}}^K} \sum_{m=1}^K \frac{P_{\text{out}}^{m-1} - P_{\text{out}}^K}{K - m + 1}. \quad (34)$$

The global gradient deviation G_{gl} can be obtained from Lemma 3 by substituting the results in Lemma 5 and 6, where we emphasize that $\Pr(k \in \mathcal{M}) = 1 - P_{\text{out}}$ and

$$\mathbb{E} \left[\sum_{k \in \mathcal{M}} G_{10,k}^* \right] = \sum_{k=1}^K \mathbb{E} [\mathbb{I}_{k \in \mathcal{M}} G_{10,k}^*] = \sum_{k=1}^K \Pr(k \in \mathcal{M}) \mathbb{E} [G_{10,k}^* | k \in \mathcal{M}]. \quad (35)$$

Then substituting G_{gl} into Proposition 1 completes the proof.

Using the preceding results, the optimal learning-energy tradeoff for the case of beacon-WPT can be readily derived as shown in the following theorem.

Theorem 1. (*Convergence with Beacon-WPT*). Consider the case of beacon-WPT. Given the optimal local computation in Section IV-A, the convergence rate of WP-FEEL is bounded by

$$\mathbb{E} \left[\frac{1}{N} \sum_{i=0}^{N-1} \|\nabla F(\mathbf{w}^{(i)})\|^2 \right] \leq \frac{2 [F(\mathbf{w}^{(0)}) - F_*]}{\eta N} + \frac{\delta W \overline{C}_\sigma (1 - P_{\text{out}})}{\rho^{\frac{1}{3}} K (T^{\text{cmp}})^{\frac{2}{3}} \lambda_{\text{energy}}^{\frac{1}{3}}} + R_{\text{es}}, \quad (36)$$

where λ_{energy} is the spatial-energy density, the parameter $\overline{C}_\sigma \triangleq \frac{1}{K} \sum_{k=1}^K \sigma_k^2 C_k^{\frac{1}{3}}$, the constant $\delta \triangleq \frac{4}{\alpha} B\left(\frac{2}{3}, \frac{2}{\alpha}\right) \left(\frac{(\beta-2)\nu^{\beta-2}}{\pi\beta}\right)^{\frac{1}{3}}$, the computation-outage probability P_{out} specified in Lemma 1, and the residue term R_{es} given as

$$R_{\text{es}} = 2 \left(\sum_{m=2}^K \frac{P_{\text{out}}^{m-1} - P_{\text{out}}^K}{K - m + 1} + P_{\text{out}}^2 \right) \Phi. \quad (37)$$

The three terms on the right-hand side of (36) are explained as follows. The first term represents gradient descent using the ground-truth gradients. The second term, which arises from the global gradient deviation, reflects the effects of beacon-WPT and other system parameters on the convergence rate. The effects of individual parameters are discussed as follows.

- (WPT effect). Recall that the spatial-energy density, $\lambda_{\text{energy}} = \bar{P} \lambda_{\text{pb}} T$, refers to the amount of energy transferred by the power-beacon network to a unit area in a single round. Increasing the density leads to a linear growth of energy harvested by each device. As a result, active devices can estimate the local gradient with higher accuracies by using larger mini-batch sizes. This leads to the decrease of the global gradient deviation proportionally with $\lambda_{\text{energy}}^{-\frac{1}{3}}$.
- (Local-computation properties). The computation parameters are grouped in $\frac{W \overline{C}_\sigma}{(T^{\text{cmp}})^{\frac{2}{3}}}$. It can be interpreted as the reduction of global gradient deviation by processing a single sample at each device. The interpretation can be derived mathematically by writing

$$\frac{W \overline{C}_\sigma}{(T^{\text{cmp}})^{\frac{2}{3}}} = \frac{1}{K} \sum_{k=1}^K \sigma_k^2 \left[\frac{C_k W^3}{(T^{\text{cmp}})^2} \right]^{\frac{1}{3}} \triangleq \frac{1}{K} \sum_{k=1}^K \sigma_k^2 (e_k^{\text{cmp}})^{\frac{1}{3}}, \quad (38)$$

where e_k^{cmp} represents the required energy for per-sample computation at device k . While the above quantity quantifies the per-sample gain of distributed gradient estimation, the number of samples each device is capable of processing depends on the spatial-energy density of beacon-WPT discussed earlier.

- (Number of devices). Due to the averaging operation in (9), increasing the number of devices, K , reduces the global gradient deviation following the scaling law of $O\left(\frac{1}{K}\right)$.

- (Probability of participation). The quantity $(1 - P_{\text{out}})$ represents the probability of participating in learning by each device. As adding an active device contributes its local gradient deviation to the global counterpart, increasing $(1 - P_{\text{out}})$ seems to enlarge the latter. On the contrary, aligned with intuition, the overall effect is to reduce the global gradient deviation if taking into account the last term, R_{es} , which is also part of the deviation and decreases as $(1 - P_{\text{out}})$ grows.

The last term R_{es} captures the loss of convergence rate caused by those devices in computation-outage. If P_{out} is small, R_{es} scales as $O(P_{\text{out}})$, confirming the effect mentioned above that R_{es} decreases as the probability of participation, $(1 - P_{\text{out}})$, grows.

The mentioned effect of WPT on the convergence of WP-FEEL can be mathematically quantified in the following corollary of Theorem 1.

Corollary 2. (*Effect of WPT*). Consider the case of beacon-WPT. As the spatial-energy density λ_{energy} grows, the convergence rate increases as follows:

$$\mathbb{E} \left[\frac{1}{N} \sum_{i=0}^{N-1} \|\nabla F(\mathbf{w}^{(i)})\|^2 \right] \leq \frac{2 [F(\mathbf{w}^{(0)}) - F_*]}{\eta N} + \Upsilon \lambda_{\text{energy}}^{-\frac{1}{3}} + O(\lambda_{\text{energy}}^{-L}), \quad \lambda_{\text{energy}} \rightarrow \infty, \quad (39)$$

where the parameter $\Upsilon \triangleq \frac{\delta W \overline{C}_\sigma}{\rho^{\frac{1}{3}} K (T^{\text{cmp}})^{\frac{2}{3}}}$, and the outage probability scales as $P_{\text{out}} = O(\lambda_{\text{energy}}^{-L})$.

V. EXTENSION TO SERVER-WPT

The preceding sections focus on beacon-WPT. The results therein can be extended to the case of server-WPT by accounting for fading in WPT links. Given channel-state information, the power allocation at the server for transfer to difference devices can be optimized in the sequel.

A. Optimal Learning-WPT Tradeoff

In the scenario of server-WPT with fading in the WPT links, the convergence analysis is more tedious than the beacon-WPT counterpart. Specifically, the current analysis differs from its beacon-WPT counterpart in two factors: 1) computation-outage probability accounting for fading in a WPT link, and 2) harvested energy that is now random. For tractability, assume equal power allocation WPT, namely that each energy beam has fixed power of P_0 (Section V-B for power control). First, the computation-outage probability, denoted as P'_{out} , is derived as follows. The

definition of a computation-outage event can be modified from that in Definition 3 by replacing \bar{E} with $E_k(r_k^{(i)}, \|\tilde{\mathbf{h}}_k^{(i)}\|^2)$. Specifically, a computation-outage event occurs if

$$\frac{\|\tilde{\mathbf{h}}_k^{(i)}\|^2 \|\mathbf{h}_k^{(i)}\|^2}{(r_k^{(i)})^{2\alpha}} \leq \frac{\varphi(T^{\text{cmm}})}{\rho P_0 T}. \quad (40)$$

To simplify notation, we define the product random variable $X = \|\tilde{\mathbf{h}}_k^{(i)}\|^2 \|\mathbf{h}_k^{(i)}\|^2$. Since both variables in the product follow the χ^2 -distribution with $2L$ degrees-of-freedom, X has the following distribution:

$$f_X(x) = \int_0^\infty f_{\|\tilde{\mathbf{h}}_k\|^2}(h) f_{\|\mathbf{h}_k\|^2}(x/h) \frac{1}{h} dh = \frac{2x^{L-1} \text{K}_0(2\sqrt{x})}{\Gamma(L)^2}, \quad (41)$$

where $\text{K}_0(\cdot)$ is the modified Bessel function of the second kind. Combining (40) and (41) gives

$$P'_{\text{out}} = \int_0^\tau \frac{2x^{L-1} \text{K}_0(2\sqrt{x}) \left(1 - (x/\tau)^{\frac{1}{\alpha}}\right)}{\Gamma(L)^2} dx, \quad (42)$$

where the parameter τ is defined as $\tau \triangleq \frac{R^{2\alpha} \varphi(T^{\text{cmm}})}{\rho P_0 T^{\text{cmp}}}$. As the exact expression of P'_{out} has no closed form, we derive an upper bound for tractability.

Corollary 3. For large transferred power ($P_0 \gg 1$), the computation-outage probability in the case of server-WPT can be bounded as:

$$P'_{\text{out}} \leq \frac{\tau^L}{\Gamma(L)^2 L(1 + \alpha L)} \ln \frac{1}{\tau} + O(P_0^{-L}). \quad (43)$$

Proof: See Appendix E. □

Given the above result, the proof of Theorem 1 can be straightforwardly extended to the current case by modifying the expressions of computation-outage probability and harvested energy, yielding the following main result of this section.

Theorem 2. (*Convergence with Server-WPT*). Consider the case of server-WPT. If the transmission power for WPT to each device is large ($P_0 \gg 1$), the convergence rate of WP-FEEL is bounded as

$$\mathbb{E} \left[\frac{1}{N} \sum_{i=0}^{N-1} \|\nabla F(\mathbf{w}^{(i)})\|^2 \right] \leq \frac{2[F(\mathbf{w}^{(0)}) - F_*]}{\eta N} + \frac{\tilde{\delta} W \overline{C}_\sigma}{\rho^{\frac{1}{3}} K T^{\text{cmp}} P_0^{\frac{1}{3}}} + O(P_0^{-L} \ln P_0), \quad P_0 \rightarrow \infty, \quad (44)$$

where the constant $\tilde{\delta}$ is defined as $\tilde{\delta} = \frac{2B(\frac{2}{3}, \frac{1}{6} + \frac{1}{\alpha}) \Gamma(L + \frac{1}{3}) R^{\frac{8}{3}}}{\alpha \Gamma(L)}$, and the upper-bound of the computation-outage probability P'_{out} as shown in (43) scales as $O(P_0^{-L} \ln P_0)$.

Comparing Theorems 1 and 2, the convergence-rate bound for server-WPT has a similar form as that for beacon-WPT except for two differences. First, the spatial energy density in the latter is replaced with transmission energy per-round for WPT, $P_0 T^{\text{cmp}}$. Second, the scaling law of the last (residual) term in (44) differs from that in (36) due to WPT-link fading. The effects of other parameters are identical to those discussed in Section IV-B.

B. Optimizing Server-WPT

The fixed power allocation for WPT in the preceding sub-section can be relaxed to improve the convergence performance. While more sophisticated designs are possible (e.g., involving optimization of the number of active devices), we consider the following practical two-step scheme to be applied in each round (with the index i omitted in the sequel to simplify notation).

- **Step 1** (Scheduling): Let \tilde{P}_k denote the power allocated for WPT to device k . Considering equal power allocation ($\tilde{P}_k = P_0$), select the set of active devices, \mathcal{M}' , by applying the computation-outage criterion in (40).
- **Step 2** (Optimal Power Control): Given \mathcal{M}' and the number of active devices $M' = |\mathcal{M}'|$, optimize the power allocation under the sum power constraint $\sum_{k \in \mathcal{M}'} \tilde{P}_k \leq M' P_0$ to minimize sum-local-gradient deviation.

For Step 2, given \mathcal{M}' and (30), the sum-local-gradient deviation is given as

$$\sum_{k \in \mathcal{M}'} G_{\text{lo},k}^* = \frac{W}{(T^{\text{cmp}})^{\frac{2}{3}}} \sum_{k \in \mathcal{M}'} \frac{\sigma_k^2 C_k^{\frac{1}{3}}}{(E_k^{\text{cmp}})^{\frac{1}{3}}}. \quad (45)$$

By substituting $\{E_k^{\text{cmp}}\}$ into (45), the problem of optimal power control can be formulated as

$$\begin{aligned} (\mathbf{P3}) \quad & \min_{\{\tilde{P}_k\}} \frac{W}{(T^{\text{cmp}})^{\frac{2}{3}}} \sum_{k \in \mathcal{M}'} \frac{\sigma_k^2 C_k^{\frac{1}{3}}}{\left(\frac{\rho \|\tilde{\mathbf{h}}_k\|^2 \tilde{P}_k T^{\text{cmp}}}{r_k^\alpha} - \frac{r_k^\alpha \varphi(T^{\text{cmm}})}{\|\mathbf{h}_k\|^2} \right)^{\frac{1}{3}}} \\ & \text{s.t.} \quad \sum_{k \in \mathcal{M}'} \tilde{P}_k \leq M' P_0. \end{aligned}$$

By a straightforward application of the KKT conditions, the optimal power-allocation policy is derived in closed-form as:

$$\tilde{P}_k^* = \frac{r_k^{2\alpha} \varphi(T^{\text{cmm}})}{\rho \|\tilde{\mathbf{h}}_k\|^2 \|\mathbf{h}_k\|^2 T^{\text{cmp}}} + \frac{r_k^{\frac{\alpha}{4}} \sigma_k^{\frac{3}{2}} C_k^{\frac{1}{4}}}{\|\tilde{\mathbf{h}}_k\|^{\frac{1}{2}} \theta} (P_0 - \varsigma), \quad \forall k \in \mathcal{M}', \quad (46)$$

where

$$\theta = \frac{1}{M'} \sum_{k \in \mathcal{M}} \frac{r_k^{\frac{\alpha}{4}} \sigma_k^{\frac{3}{2}} C_k^{\frac{1}{4}}}{\|\tilde{\mathbf{h}}_k\|^{\frac{1}{2}}} \quad \text{and} \quad \varsigma = \frac{1}{M'} \sum_{k \in \mathcal{M}} \frac{r_k^{2\alpha} \varphi(T^{\text{cmm}})}{\rho \|\tilde{\mathbf{h}}_k\|^2 \|\mathbf{h}_k\|^2 T^{\text{cmp}}}, \quad (47)$$

and thus omitted for brevity. One can observe from (46) that the optimal power allocated for WPT sums two components. The first component, which supports gradient uploading, is inversely proportional to the gain of the close-loop channel cascading downlink for WPT and uplink for gradient uploading. The other component, which supports local computation, depends only on the WPT link and is a monotone decreasing function of the channel gain of the WPT link.

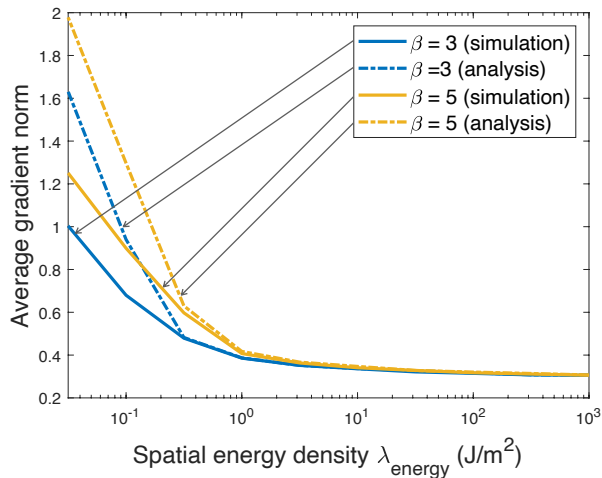
VI. EXPERIMENTAL RESULTS

A. Experimental Settings

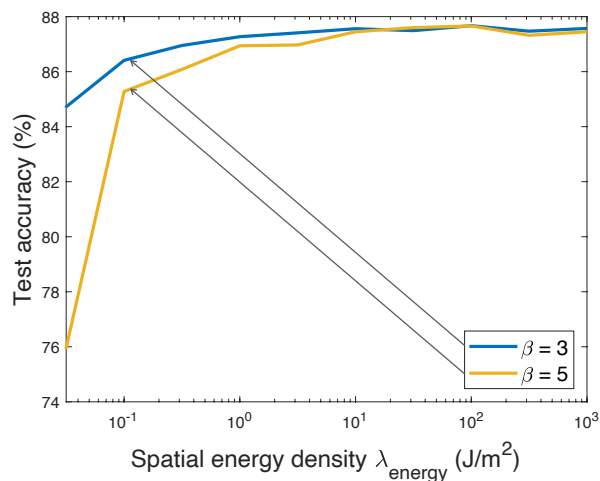
The default settings are as follows. The edge server is equipped with 64 antennas and the cell radius is set as $R = 100$ m. There are $K = 30$ edge devices uniformly distributed in the cell, each of which is allocated an uplink bandwidth $B = 1$ MHz. The noise spectrum density is $N_0 = -80$ dBm/Hz and the path loss exponents are $\alpha = 3.8$ and $\beta = 4$. For the WPT path-loss model, $\nu = 1$. The processor coefficients $\{C_k\}$ are chosen by uniformly sampling the set $\{0.010, 0.011, \dots, 0.100\}$ [in $\text{Watt} \cdot (\text{MFLOPs/s})^{-3}$]. The learning task aims at training a CNN model to classify handwritten digits using the well-known MNIST dataset. For non-i.i.d. data distribution, we first arrange 6×10^4 data samples according to their labels, follow the sample sequence to divide the dataset into 60 subsets each of size 1000, and assign each of 30 devices 2 data subsets. The classifier model is implemented using a 6-layer CNN which consists of two 5×5 convolution layers with ReLU activation, each followed by 2×2 max pooling, a fully connected layer with 50 units and ReLU activation, and a final softmax output layer. The total number of parameters is $q = 21,840$ and the per-sample computation workload is $W = 1.09 \times 10^6$ FLOPs. Furthermore, we suppose that each parameter of the training model gradient is quantized into $Q = 16$ bits, and as a result, the transmission overhead in one round is 3.49×10^5 bits. We fix the number of rounds as $N = 500$ and evaluate the learning performance in terms of average gradient norm (over rounds) and test accuracy.

B. Performance of WP-FEEL with Beacon-WPT

The curves of learning performance versus the spatial-energy density λ_{energy} provided by the power-beacon network are plotted in Fig. 3 for a varying path-loss exponent of WPT links, β . Both experimental and analytical results are presented. Several observations can be made. As λ_{energy} grows, the increase of transferred energy allows more devices to participate in learning or equivalently more distributed data to be exploited for model training. Consequently, one can



(a) Average gradient norm

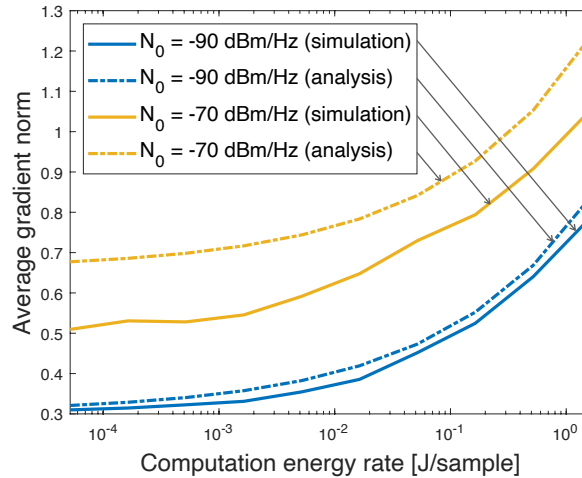


(b) Test accuracy

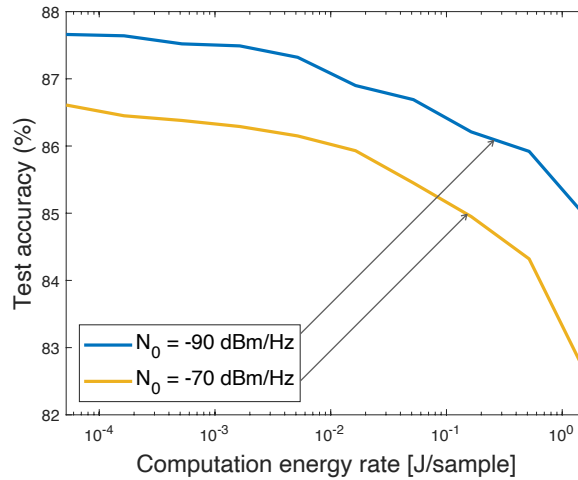
Figure 3. Effects of the spatial-energy density on the performance of a WP-FEEL system with beacon-WPT.

observe that both the average gradient norm and test accuracy saturate as they converge to their ground-truths. Next, before the convergence, the average gradient norms from analysis and experiments follow the same scaling laws. That validates the analytical model and the results in Theorem 1 and its corollary. Last, one can observe that a larger value of β and hence smaller path loss results in better performance as more energy can be transferred from beacons to devices.

Define the computation-energy rate of a device as the number of FLOPs computed by its processor per unit energy consumption. For ease of exposition, consider the case of uniform computation-energy rates for all devices. The curves of learning performance versus computation-energy rates are plotted in Fig. 4 for a varying noise power spectrum density N_0 . Several



(a) Average gradient norm



(b) Test accuracy

Figure 4. Effects of computation energy consumption and channel noise on the performance of a WP-FEEL system with beacon-WPT.

observations can be made. Both the analytical and experiment results are presented in the figure. Their discrepancy arises from some mismatch between the general analytical model specified in the common Assumptions 1–4 and the specific dataset (i.e., MNIST) used in the experiments. The mismatch is observed to less for smaller N_0 due to the averaging effect of more devices/more data involved in learning. Next, aligned with intuition, reducing N_0 improves learning performance by activating more devices as well as reducing the communication-energy consumption; thereby more energy is allowed for local gradient estimation and its accuracy improves. Next, given fixed harvested energy per device, one can observe degradation of learning performance as the

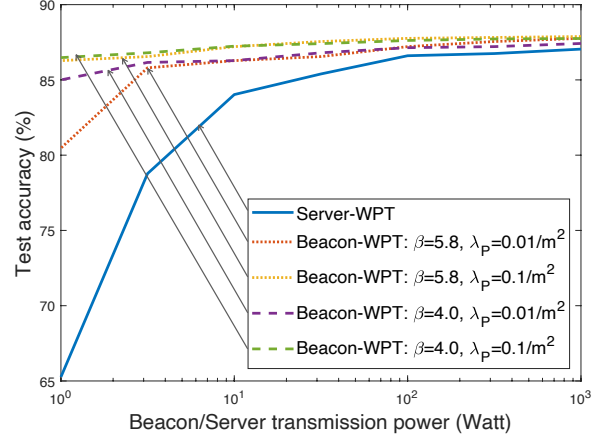
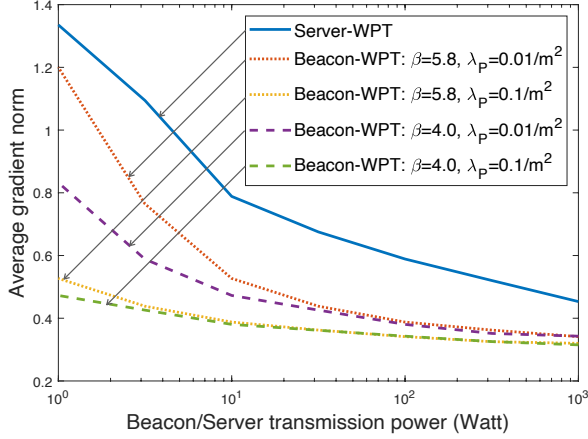
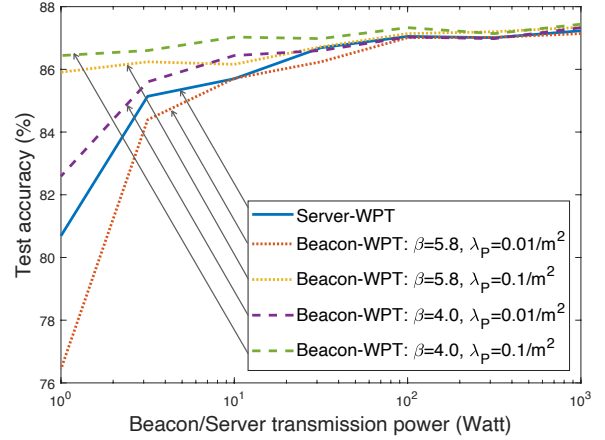
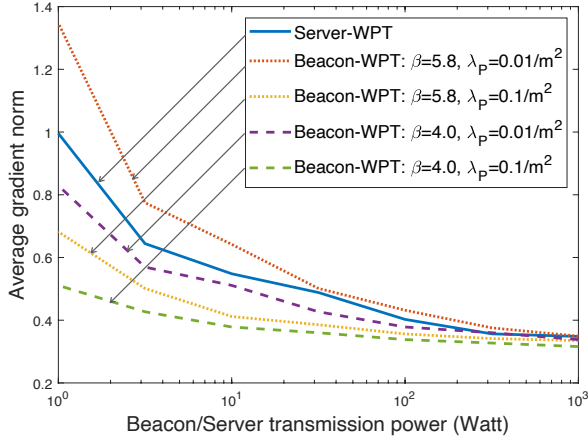
(a) Cell radius $R = 20$ m.(b) Cell radius $R = 10$ m.

Figure 5. Learning-performance comparison between beacon-WPT and server-WPT.

increasing computation-energy rate reduces the mini-batch size, the number of active devices, and the energy available for communication.

C. Comparison between Beacon-WPT and Server-WPT

Based on experiments, the learning performance for the scenarios of beacon-WPT and server-WPT is compared in Fig. 5 for two different cell sizes. For the purpose of comparison, the transmission power of power-beacons and serve are equalized $\bar{P} = P_0$ while the beacon density, λ_{pb} , and the path-loss exponent of beacon-WPT links, β , are varied. For a relatively large cell ($R = 20$ m), it can be observed that beacon-WPT always outperforms server-WPT in the considered ranges of settings as the latter with only a single power source suffers from a low WPT efficiency due to severe path loss. This suggests the need of deploying power-beacons

to power devices if FEEL is deployed in a large area to involve many devices. On the other hand, for a relatively small cell ($R = 10$ m), server-WPT has a higher WPT efficiency and can outperform beacon-WPT when beacons are sparse and/or the path-loss exponent β is large.

VII. CONCLUDING REMARKS

In this paper, we have proposed the application of WPT to a FEEL system as a solution for the practical issue of high energy consumption at devices. To study the performance of the resultant WP-FEEL system, we have analyzed the optimal learning-WPT tradeoffs for both the scenarios of beacon-WPT and server-WPT. The results contribute useful insight and algorithms for designing and deploying WP-FEEL systems. This first study of WP-FEEL opens several directions for further research including the application of WPT to support the implementation of other edge-learning frameworks (e.g., parameter server and reinforcement learning), the use of more complex wireless techniques (e.g., over-the-air aggregation and radio resource management), and the design of multi-cell networks.

APPENDIX

A. Proof of Proposition 1

According to the update rule in (10) and Assumption 1, we have

$$\begin{aligned} F(\mathbf{w}^{(i+1)}) - F(\mathbf{w}^{(i)}) &\leq \langle \nabla F(\mathbf{w}^{(i)}), \mathbf{w}^{(i+1)} - \mathbf{w}^{(i)} \rangle + \frac{\mu}{2} \|\mathbf{w}^{(i+1)} - \mathbf{w}^{(i)}\|^2 \\ &= -\eta \langle \nabla F(\mathbf{w}^{(i)}), \mathbf{g}^{(i)} \rangle + \frac{\mu\eta^2}{2} \|\mathbf{g}^{(i)}\|^2. \end{aligned} \quad (48)$$

Using $\|\mathbf{g}^{(i)}\|^2 = \|\mathbf{g}^{(i)} - \nabla F(\mathbf{w}^{(i)})\|^2 - \|\nabla F(\mathbf{w}^{(i)})\|^2 + 2\langle \nabla F(\mathbf{w}^{(i)}), \mathbf{g}^{(i)} \rangle$, we can derive

$$\begin{aligned} F(\mathbf{w}^{(i+1)}) - F(\mathbf{w}^{(i)}) &\leq \frac{\mu\eta^2}{2} (\|\mathbf{g}^{(i)} - \nabla F(\mathbf{w}^{(i)})\|^2 - \|\nabla F(\mathbf{w}^{(i)})\|^2) + (\mu\eta - 1)\eta \langle \nabla F(\mathbf{w}^{(i)}), \mathbf{g}^{(i)} \rangle \\ &= \frac{\mu\eta^2}{2} \|\mathbf{g}^{(i)} - \nabla F(\mathbf{w}^{(i)})\|^2 + \left(\frac{\mu\eta}{2} - 1\right) \eta \|\nabla F(\mathbf{w}^{(i)})\|^2 \\ &\quad - (1 - \mu\eta)\eta \langle \nabla F(\mathbf{w}^{(i)}), \mathbf{g}^{(i)} - \nabla F(\mathbf{w}^{(i)}) \rangle. \end{aligned} \quad (49)$$

The third term at the right-hand side in (49) can be upper bounded as

$$-\langle \nabla F(\mathbf{w}^{(i)}), \mathbf{g}^{(i)} - \nabla F(\mathbf{w}^{(i)}) \rangle \leq \frac{1}{2} (\|\nabla F(\mathbf{w}^{(i)})\|^2 + \|\mathbf{g}^{(i)} - \nabla F(\mathbf{w}^{(i)})\|^2). \quad (50)$$

Given $0 < \eta \leq \frac{1}{\mu}$, we substitute (50) into (49) and rearrange the result, yielding

$$\|\nabla F(\mathbf{w}^{(i)})\|^2 \leq \frac{2(F(\mathbf{w}^{(i)}) - F(\mathbf{w}^{(i+1)}))}{\eta} + \|\mathbf{g}^{(i)} - \nabla F(\mathbf{w}^{(i)})\|^2. \quad (51)$$

It follows that

$$\begin{aligned} \mathbb{E} \left[\frac{1}{N} \sum_{i=0}^{N-1} \|\nabla F(\mathbf{w}^{(i)})\|^2 \right] &\leq \frac{2(F(\mathbf{w}^{(0)}) - \mathbb{E}[F(\mathbf{w}^{(N)})])}{\eta N} + \frac{1}{N} \sum_{i=0}^{N-1} \mathbb{E} [\|\mathbf{g}^{(i)} - \nabla F(\mathbf{w}^{(i)})\|^2] \\ &\leq \frac{2(F(\mathbf{w}^{(0)}) - F_*)}{\eta N} + \frac{1}{N} \sum_{i=0}^{N-1} \mathbb{E} [\|\mathbf{g}^{(i)} - \nabla F(\mathbf{w}^{(i)})\|^2], \end{aligned} \quad (52)$$

where the second inequality in (52) follows Assumption 3. This completes the proof.

B. Proof of Lemma 3

The aggregated global gradient can be written using the indicator function \mathbb{I} as

$$\mathbf{g} = \frac{1}{M} \sum_{k \in \mathcal{M}} \mathbf{g}_k = \frac{1}{M} \sum_{k=1}^K \mathbb{I}_{k \in \mathcal{M}} \mathbf{g}_k, \text{ if } M > 0; \text{ and } \mathbf{g} = \mathbf{0}, \text{ otherwise.} \quad (53)$$

For tractability, we introduce the following auxiliary gradient $\tilde{\mathbf{g}}$ which is defined by

$$\tilde{\mathbf{g}} = \frac{1}{K} \sum_{k=1}^K \mathbb{I}_{k \in \mathcal{M}} \mathbf{g}_k, \text{ where } \mathbb{I}_{k \in \mathcal{M}} \mathbf{g}_k = 0 \text{ for } k \in \mathcal{K} \setminus \mathcal{M}. \quad (54)$$

Then, we can derive the following upper bound for G_{gl} using the auxiliary gradient:

$$G_{\text{gl}} = \mathbb{E}_{\mathcal{M}} \left\{ \mathbb{E} [\|\tilde{\mathbf{g}} - \nabla F(\mathbf{w}) + \mathbf{g} - \tilde{\mathbf{g}}\|^2] \right\} \leq 2 \mathbb{E}_{\mathcal{M}} \left\{ \underbrace{\mathbb{E} [\|\tilde{\mathbf{g}} - \nabla F(\mathbf{w})\|^2]}_{(a)} + \underbrace{\mathbb{E} [\|\mathbf{g} - \tilde{\mathbf{g}}\|^2]}_{(b)} \right\}. \quad (55)$$

In the following, we focus on terms (a) and (b) defined in (55), respectively.

- 1) Since $\nabla F(\mathbf{w}) = \frac{1}{K} \sum_{k=1}^K \nabla F_k(\mathbf{w})$, we can first decompose term (a) as follows:

$$\begin{aligned} \text{(a)} &= \mathbb{E} [\|\tilde{\mathbf{g}} - \nabla F(\mathbf{w})\|^2] = \frac{1}{K^2} \sum_{k=1}^K \sum_{\ell=1}^K \mathbb{E} [\langle \mathbb{I}_{k \in \mathcal{M}} \mathbf{g}_k - \nabla F_k(\mathbf{w}), \mathbb{I}_{\ell \in \mathcal{M}} \mathbf{g}_\ell - \nabla F_\ell(\mathbf{w}) \rangle] \\ &= \frac{1}{K^2} \left(\underbrace{\sum_{k=1}^K \mathbb{E} [\|\mathbb{I}_{k \in \mathcal{M}} \mathbf{g}_k - \nabla F_k(\mathbf{w})\|^2]}_{(a1)} + \underbrace{\sum_{k \neq \ell} \mathbb{E} [\langle \mathbb{I}_{k \in \mathcal{M}} \mathbf{g}_k - \nabla F_k(\mathbf{w}), \mathbb{I}_{\ell \in \mathcal{M}} \mathbf{g}_\ell - \nabla F_\ell(\mathbf{w}) \rangle]}_{(a2)} \right), \end{aligned}$$

Next, we aim at finding the upper bounds for terms (a1) and (a2), respectively.

- For term (a1), we can bound it as follows:

$$\begin{aligned} \text{(a1)} &= \sum_{k=1}^K \mathbb{I}_{k \in \mathcal{M}} \mathbb{E} [\|\mathbf{g}_k - \nabla F_k(\mathbf{w})\|^2] + \sum_{k=1}^K \mathbb{I}_{k \in \mathcal{K} \setminus \mathcal{M}} \{ \mathbb{E} [\|\nabla F_k(\mathbf{w})\|^2] \} \\ &\leq \sum_{k=1}^K \mathbb{I}_{k \in \mathcal{M}} G_{10,k} + (K - M) \Phi, \end{aligned} \quad (56)$$

which comes from Jensen's inequality $\|\nabla F_k(\mathbf{w})\|^2 = \|\mathbb{E}[\mathbf{g}_k]\|^2 \leq \mathbb{E}[\|\mathbf{g}_k\|^2] \leq \Phi$. Then,

$$\mathbb{E}_{\mathcal{M}}[(a1)] \leq \mathbb{E}\left[\sum_{k \in \mathcal{M}} G_{10,k}\right] + (K - \mathbb{E}[M])\Phi. \quad (57)$$

- For term (a2), we can first divide $\mathbb{E}[\langle \mathbb{I}_{k \in \mathcal{M}} \mathbf{g}_k - \nabla F_k(\mathbf{w}), \mathbb{I}_{\ell \in \mathcal{M}} \mathbf{g}_\ell - \nabla F_\ell(\mathbf{w}) \rangle]$ into three categories ($k \neq \ell$):

- i) Case 1: $k \in \mathcal{M}$ and $\ell \in \mathcal{M}$. Given Assumption 2, \mathbf{g}_k and \mathbf{g}_ℓ are uncorrelated, so

$$\begin{aligned} & \mathbb{E}[\langle \mathbb{I}_{k \in \mathcal{M}} \mathbf{g}_k - \nabla F_k(\mathbf{w}), \mathbb{I}_{\ell \in \mathcal{M}} \mathbf{g}_\ell - \nabla F_\ell(\mathbf{w}) \rangle] \\ &= \mathbb{E}[(\mathbf{g}_k - \nabla F_k(\mathbf{w}))^\top (\mathbf{g}_\ell - \nabla F_\ell(\mathbf{w}))] = \text{tr}\{\text{cov}(\mathbf{g}_k, \mathbf{g}_\ell)\} = 0. \end{aligned} \quad (58)$$

- ii) Case 2: $k \in \mathcal{M}$ but $\ell \notin \mathcal{M}$ (or $k \notin \mathcal{M}$ but $\ell \in \mathcal{M}$). Given Assumption 2, \mathbf{g}_k is an unbiased estimate of $\nabla F_k(\mathbf{w})$, resulting in

$$\mathbb{E}[\langle \mathbb{I}_{k \in \mathcal{M}} \mathbf{g}_k - \nabla F_k(\mathbf{w}), \mathbb{I}_{\ell \in \mathcal{M}} \mathbf{g}_\ell - \nabla F_\ell(\mathbf{w}) \rangle] = -\mathbb{E}[(\mathbf{g}_k - \nabla F_k(\mathbf{w}))^\top \nabla F_\ell(\mathbf{w})] = 0. \quad (59)$$

- iii) Case 3: $k \notin \mathcal{M}$ and $\ell \notin \mathcal{M}$. When both device k and ℓ are outage, it holds

$$\mathbb{E}[\langle \mathbb{I}_{k \in \mathcal{M}} \mathbf{g}_k - \nabla F_k(\mathbf{w}), \mathbb{I}_{\ell \in \mathcal{M}} \mathbf{g}_\ell - \nabla F_\ell(\mathbf{w}) \rangle] = \nabla F_k(\mathbf{w})^\top \nabla F_\ell(\mathbf{w}). \quad (60)$$

Combining the above three cases, we can bound term (a2) as follows:

$$\begin{aligned} (a2) &= \sum_{k \neq \ell} \mathbb{I}_{k \notin \mathcal{M}} \mathbb{I}_{\ell \notin \mathcal{M}} \langle \nabla F_k(\mathbf{w}), \nabla F_\ell(\mathbf{w}) \rangle \\ &\leq \sum_{k \neq \ell} \mathbb{I}_{k \notin \mathcal{M}} \mathbb{I}_{\ell \notin \mathcal{M}} \|\nabla F_k(\mathbf{w})\| \|\nabla F_\ell(\mathbf{w})\| \leq \sum_{k \neq \ell} \mathbb{I}_{k \notin \mathcal{M}} \mathbb{I}_{\ell \notin \mathcal{M}} \Phi. \end{aligned} \quad (61)$$

Then, taking expectation over \mathcal{M} , we can obtain

$$\mathbb{E}_{\mathcal{M}}[(a2)] \leq \mathbb{E}\left[\sum_{k \neq \ell} \mathbb{I}_{k \notin \mathcal{M}} \mathbb{I}_{\ell \notin \mathcal{M}}\right] \Phi = (K^2 - K)P_{\text{out}}^2 \Phi. \quad (62)$$

In summary, the expected term (a) in (55) can be upper bounded by

$$\mathbb{E}_{\mathcal{M}}[(a)] \leq \frac{1}{K^2} \mathbb{E}\left[\sum_{k \in \mathcal{M}} G_{10,k}\right] + \frac{K - \mathbb{E}[M]}{K^2} \Phi + \frac{K - 1}{K} P_{\text{out}}^2 \Phi. \quad (63)$$

- 2) For term (b) in (55), we can derive the upper bound as follows:

$$\begin{aligned} (b) &= \mathbb{E}[\|\mathbf{g} - \tilde{\mathbf{g}}\|^2] = \mathbb{I}_{M>0} \mathbb{E}\left[\left\|\left(\frac{1}{M} - \frac{1}{K}\right) \sum_{k \in \mathcal{M}} \mathbf{g}_k\right\|^2\right] + \mathbb{I}_{M=0} \times 0 \\ &\leq \mathbb{I}_{M>0} \left(\frac{1}{M} - \frac{1}{K}\right)^2 \sum_{k \in \mathcal{M}} \mathbb{E}[\|\mathbf{g}_k\|^2] \leq \mathbb{I}_{M>0} \left(\frac{1}{M} + \frac{M}{K^2} - \frac{2}{K}\right) \Phi, \end{aligned} \quad (64)$$

where we note that, when $M = 0$, both \mathbf{g} and $\tilde{\mathbf{g}}$ are zero, thus $\mathbb{E}[\|\mathbf{g} - \tilde{\mathbf{g}}\|^2 | M = 0] = 0$.

Furthermore, considering

$$\mathbb{E}[M] = \Pr(M > 0)\mathbb{E}[M | M > 0] + \Pr(M = 0)\mathbb{E}[M | M = 0] = \Pr(M > 0)\mathbb{E}[M | M > 0]$$

and $\Pr(M > 0) = 1 - P_{\text{out}}^K$, we can bound the expected (b) as

$$\begin{aligned} \mathbb{E}_{\mathcal{M}}[(\mathbf{b})] &\leq \Pr(M > 0)\mathbb{E}\left[\frac{1}{M} + \frac{M}{K} - \frac{2}{K} \middle| M > 0\right] \Phi \\ &= \left((1 - P_{\text{out}}^K)\mathbb{E}\left[\frac{1}{M} \middle| M > 0\right] + \frac{1}{K^2}\mathbb{E}[M] - (1 - P_{\text{out}}^K)\frac{2}{K}\right) \Phi. \end{aligned} \quad (65)$$

Finally, substituting the results (63) and (65) into (55), we have

$$\begin{aligned} \frac{1}{2}G_{\text{gl}} &\leq \frac{1}{K^2}\mathbb{E}\left[\sum_{k \in \mathcal{M}} G_{10,k}\right] + (1 - P_{\text{out}}^K)\left(\mathbb{E}\left[\frac{1}{M} \middle| M > 0\right] - \frac{1}{K}\right) \Phi + \frac{P_{\text{out}}^K - P_{\text{out}}^2}{K} + P_{\text{out}}^2 \Phi \\ &\leq \frac{1}{K^2}\mathbb{E}\left[\sum_{k \in \mathcal{M}} G_{10,k}\right] + (1 - P_{\text{out}}^K)\left(\mathbb{E}\left[\frac{1}{M} \middle| M > 0\right] - \frac{1}{K}\right) \Phi + P_{\text{out}}^2 \Phi, \end{aligned} \quad (66)$$

where we note that $P_{\text{out}}^K - P_{\text{out}}^2 \leq 0$ due to $K \geq 2$. This completes the proof.

C. Proof of Lemma 1

According to Definition 3, in the i -th round, the device k encounters a computation-outage event if the condition $E_k^{\text{cmm}}(r_k^{(i)}, \mathbf{h}_k^{(i)}) \geq \bar{E}$, which is equivalent to $R^\alpha \|\mathbf{h}_k^{(i)}\|^2 \leq \left(r_k^{(i)}\right)^\alpha \frac{\varphi(T^{\text{cmm}})}{R^{-\alpha} \bar{E}}$, is true. Define the domain $\Xi = \{(r, h) \in \mathbb{R}^2 : R^\alpha h \leq r^\alpha \xi; h \geq 0; 0 \leq r \leq R\}$ for inactive devices, where ξ has the same definition as mentioned in (25). Since $\mathbf{h}_k^{(i)}$ and $r_k^{(i)}$ are independent, we know $f_{(r_k^{(i)}, \|\mathbf{h}_k^{(i)}\|^2)}(r, h) = f_{\|\mathbf{h}_k^{(i)}\|^2}(h) f_{r_k^{(i)}}(r)$. Then, we can derive the outage probability:

$$\begin{aligned} P_{\text{out}} &= \iint_{\Xi} f_{\|\mathbf{h}_k^{(i)}\|^2}(h) f_{r_k^{(i)}}(r) dr dh = \int_0^R \frac{2r}{R^2} \int_0^{\left(\frac{r}{R}\right)^\alpha \xi} \frac{h^{L-1} e^{-h}}{\Gamma(L)} dh dr \\ &= \frac{2}{R^2 \Gamma(L)} \int_0^R \gamma\left(L, \left(\frac{r}{R}\right)^\alpha \xi\right) r dr = \frac{\gamma(L, \xi) - \xi^{-\frac{2}{\alpha}} \gamma\left(L + \frac{2}{\alpha}, \xi\right)}{\Gamma(L)}. \end{aligned} \quad (67)$$

This completes the proof.

D. Proof of Lemma 5

The aggregated local gradient deviations come from the active devices. Define the domain $\Theta = \{(r, h) \in \mathbb{R}^2 : R^\alpha h > r^\alpha \xi; h \geq 0; 0 \leq r \leq R\}$ for active devices, where ξ has the same definition as mentioned in (25). By variable transform, we introduce a new integral variant

$x \triangleq \left(\frac{r}{R}\right)^\alpha \xi$, so that $r = R\xi^{-\frac{1}{\alpha}}x^{\frac{1}{\alpha}}$ and $dr = \frac{1}{\alpha}R\xi^{-\frac{1}{\alpha}}x^{\frac{1}{\alpha}-1}dx$. Accordingly, the integral domain becomes $\Theta = \{(x, h) \in \mathbb{R}^2 : h > x; 0 \leq x \leq \xi\}$. Then we can obtain

$$\begin{aligned} \mathbb{E} [\mathbb{I}_{k \in \mathcal{M}} G_{10,k}^*] &= \frac{W\sigma_k^2 C_k^{\frac{1}{3}} \xi^{\frac{1}{3}}}{T^{\text{cmp}\frac{2}{3}} \varphi(T^{\text{cmm}})^{\frac{1}{3}}} \iint_{\Theta} \left(\frac{h}{R^\alpha h - r^\alpha \xi}\right)^{\frac{1}{3}} \frac{h^{L-1} e^{-h}}{\Gamma(L)} \frac{2r}{R^2} dr dh \\ &= \frac{2W\sigma_k^2 C_k^{\frac{1}{3}} \xi^{\frac{1}{3} - \frac{2}{\alpha}}}{\alpha T^{\text{cmp}\frac{2}{3}} R^{\frac{\alpha}{3}} \varphi(T^{\text{cmm}})^{\frac{1}{3}} \Gamma(L)} \underbrace{\iint_{\Theta} \frac{h^{L-\frac{2}{3}} e^{-h}}{(h-x)^{\frac{1}{3}} x^{1-\frac{2}{\alpha}}} dx dh}_{(c)}. \end{aligned} \quad (68)$$

The integration (c) defined in (68) can be decomposed into two terms as follows:

$$(c) = \underbrace{\int_0^\xi \int_0^h \frac{h^{L-\frac{2}{3}} e^{-h}}{(h-x)^{\frac{1}{3}} x^{1-\frac{2}{\alpha}}} dx dh}_{(c1)} + \underbrace{\int_\xi^\infty \int_0^\xi \frac{h^{L-\frac{2}{3}} e^{-h}}{(h-x)^{\frac{1}{3}} x^{1-\frac{2}{\alpha}}} dx dh}_{(c2)}, \quad (69)$$

1) For term (c1), we can derive the result as follows:

$$(c1) = B\left(\frac{2}{3}, \frac{2}{\alpha}\right) \int_0^\xi h^{L+\frac{2}{\alpha}-1} e^{-h} dh = B\left(\frac{2}{3}, \frac{2}{\alpha}\right) \gamma\left(L + \frac{2}{\alpha}, \xi\right). \quad (70)$$

2) For term (c2), we can find an upper bound as follows:

$$\begin{aligned} (c2) &= \int_\xi^\infty h^{L-1} e^{-h} \int_0^\xi \left(1 - \frac{x}{h}\right)^{-\frac{1}{3}} x^{\frac{2}{\alpha}-1} dx dh \\ &\leq \int_\xi^\infty h^{L-1} e^{-h} dh \int_0^\xi \left(1 - \frac{x}{\xi}\right)^{-\frac{1}{3}} x^{\frac{2}{\alpha}-1} dx = B\left(\frac{2}{3}, \frac{2}{\alpha}\right) \xi^{\frac{2}{\alpha}} \Gamma(L, \xi). \end{aligned} \quad (71)$$

Substituting the results (70) and (71) into (68), we can derive the following upper bound:

$$\mathbb{E} [\mathbb{I}_{k \in \mathcal{M}} G_{10,k}^*] \leq \frac{2W\sigma_k^2 C_k^{\frac{1}{3}} B\left(\frac{2}{3}, \frac{2}{\alpha}\right) \xi^{\frac{1}{3}}}{\alpha T^{\text{cmp}\frac{2}{3}} R^{\frac{\alpha}{3}} \varphi(T^{\text{cmm}})^{\frac{1}{3}} \Gamma(L)} \left(\xi^{-\frac{2}{\alpha}} \gamma\left(L + \frac{2}{\alpha}, \xi\right) + \Gamma(L, \xi) \right). \quad (72)$$

Expanding $\mathbb{E}[\mathbb{I}_{k \in \mathcal{M}} G_{10,k}^*]$ and comparing the right-hand side with the expression of P_{out} , we have

$$\Pr(k \in \mathcal{M}) \mathbb{E} [G_{10,k}^* | k \in \mathcal{M}] \leq \frac{2W\sigma_k^2 C_k^{\frac{1}{3}} B\left(\frac{2}{3}, \frac{2}{\alpha}\right) \xi^{\frac{1}{3}}}{\alpha T^{\text{cmp}\frac{2}{3}} R^{\frac{\alpha}{3}} \varphi(T^{\text{cmm}})^{\frac{1}{3}}} (1 - P_{\text{out}}). \quad (73)$$

Note that $\Pr(k \in \mathcal{M}) = 1 - P_{\text{out}}$ and this completes the proof.

E. Proof of Corollary 3

Applying the second mean value theorem for definite integrals, we can derive (with $\tau \ll 1$)

$$\begin{aligned} P'_{\text{out}} &= \int_0^\tau \frac{2\mathcal{K}_0(2\sqrt{x})}{\ln x} \frac{x^{L-1} \left[1 - \left(\frac{x}{\tau}\right)^{\frac{1}{\alpha}}\right] \ln x}{\Gamma(L)^2} dx \\ &= \left[\lim_{x \rightarrow 0^+} \frac{2\mathcal{K}_0(2\sqrt{x})}{\ln x} \right] \int_0^{\tau'} \frac{x^{L-1} \left[1 - \left(\frac{x}{\tau}\right)^{\frac{1}{\alpha}}\right] \ln x}{\Gamma(L)^2} dx \\ &\leq - \int_0^\tau \frac{x^{L-1} \left[1 - \left(\frac{x}{\tau}\right)^{\frac{1}{\alpha}}\right] \ln x}{\Gamma(L)^2} dx = \frac{\tau^L (1 + 2\alpha L - L(1 + \alpha L) \ln \tau)}{\Gamma(L)^2 L^2 (1 + \alpha L)^2}, \end{aligned} \quad (74)$$

where $\frac{2K_0(2\sqrt{x})}{\ln x}$ is a negative monotone increasing function around 0^+ with $\lim_{x \rightarrow 0^+} \frac{2K_0(2\sqrt{x})}{\ln x} = -1$ and the number $\tau' \in (0, \tau]$. This completes the proof.

REFERENCES

- [1] Z. Zhou, X. Chen, E. Li, L. Zeng, K. Luo, and J. Zhang, "Edge intelligence: Paving the last mile of artificial intelligence with edge computing," *Proc. IEEE*, vol. 107, no. 8, pp. 1738–1762, 2019.
- [2] G. Zhu, D. Liu, Y. Du, C. You, J. Zhang, and K. Huang, "Toward an intelligent edge: Wireless communication meets machine learning," *IEEE Commun. Mag.*, vol. 58, no. 1, pp. 19–25, 2020.
- [3] W. Y. B. Lim, N. C. Luong, D. T. Hoang, Y. Jiao, Y. C. Liang, Q. Yang, D. Niyato, and C. Miao, "Federated learning in mobile edge networks: A comprehensive survey," *IEEE Commun. Surveys Tuts.*, vol. 22, no. 3, pp. 2031–2063, 2020.
- [4] S. Wang, T. Tuor, T. Salonidis, K. K. Leung, C. Makaya, T. He, and K. Chan, "Adaptive federated learning in resource constrained edge computing systems," *IEEE J. Sel. Areas Commun.*, vol. 37, no. 6, pp. 1205–1221, 2019.
- [5] M. M. Amiri and D. Gündüz, "Machine learning at the wireless edge: Distributed stochastic gradient descent over-the-air," *IEEE Trans. Signal Process.*, vol. 68, pp. 2155–2169, 2020.
- [6] G. Zhu, Y. Wang, and K. Huang, "Broadband analog aggregation for low-latency federated edge learning," *IEEE Trans. Wireless Commun.*, vol. 19, no. 1, pp. 491–506, 2020.
- [7] K. Yang, T. Jiang, Y. Shi, and Z. Ding, "Federated learning via over-the-air computation," *IEEE Trans. Wireless Commun.*, vol. 19, no. 3, pp. 2022–2035, 2020.
- [8] M. Chen, Z. Yang, W. Saad, C. Yin, H. V. Poor, and S. Cui, "A joint learning and communications framework for federated learning over wireless networks," *IEEE Trans. Wireless Commun.*, vol. 20, no. 1, pp. 269–283, 2021.
- [9] J. Ren, G. Yu, and G. Ding, "Accelerating dnn training in wireless federated edge learning systems," *IEEE J. Sel. Areas Commun.*, vol. 39, no. 1, pp. 219–232, 2021.
- [10] D. Wen, M. Bennis, and K. Huang, "Joint parameter-and-bandwidth allocation for improving the efficiency of partitioned edge learning," *IEEE Trans. Wireless Commun.*, vol. 19, no. 12, pp. 8272–8286, 2020.
- [11] H. H. Yang, Z. Liu, T. Q. S. Quek, and H. V. Poor, "Scheduling policies for federated learning in wireless networks," *IEEE Trans. Commun.*, vol. 68, no. 1, pp. 317–333, 2020.
- [12] Y. Du, S. Yang, and K. Huang, "High-dimensional stochastic gradient quantization for communication-efficient edge learning," *IEEE Trans. Signal Process.*, vol. 68, pp. 2128–2142, 2020.
- [13] Y. Sun, S. Zhou, and D. Gündüz, "Energy-aware analog aggregation for federated learning with redundant data," in *IEEE Int. Conf. Commun. (ICC)*, Dublin, Ireland, Jun 7-11, 2020.
- [14] Z. Yang, M. Chen, W. Saad, C. S. Hong, and M. Shikh-Bahaei, "Energy efficient federated learning over wireless communication networks," *to appear in IEEE Trans. Wireless Commun.*, 2020.
- [15] X. Mo and J. Xu, "Energy-efficient federated edge learning with joint communication and computation design," [Online] <https://arxiv.org/pdf/2003.00199.pdf>, 2020.
- [16] Q. Zeng, Y. Du, K. Huang, and K. K. Leung, "Energy-efficient resource management for federated edge learning with cpu-gpu heterogeneous computing," [Online] <https://arxiv.org/pdf/2007.07122.pdf>, 2020.
- [17] B. Clerckx, R. Zhang, R. Schober, D. W. K. Ng, D. I. Kim, and H. V. Poor, "Fundamentals of wireless information and power transfer: From RF energy harvester models to signal and system designs," *IEEE J. Sel. Areas Commun.*, vol. 37, no. 1, pp. 4–33, 2019.
- [18] B. Clerckx, K. Huang, L. R. Varshney, S. Ulukus, and M.-S. Alouini, "Wireless power transfer for future networks: Signal processing, machine learning, computing, and sensing," [Online] <https://arxiv.org/pdf/2101.04810.pdf>, 2021.

- [19] K. Huang and X. Zhou, "Cutting the last wires for mobile communications by microwave power transfer," *IEEE Commun. Mag.*, vol. 53, no. 6, pp. 86–93, 2015.
- [20] R. Zhang and C. K. Ho, "Mimo broadcasting for simultaneous wireless information and power transfer," *IEEE Trans. Wireless Commun.*, vol. 12, no. 5, pp. 1989–2001, 2013.
- [21] H. Ju and R. Zhang, "Throughput maximization in wireless powered communication networks," *IEEE Trans. Wireless Commun.*, vol. 13, no. 1, pp. 418–428, 2014.
- [22] K. Huang and V. K. N. Lau, "Enabling wireless power transfer in cellular networks: Architecture, modeling and deployment," *IEEE Trans. Wireless Commun.*, vol. 13, no. 2, pp. 902–912, 2014.
- [23] Q. Wu, M. Tao, D. W. Kwan Ng, W. Chen, and R. Schober, "Energy-efficient resource allocation for wireless powered communication networks," *IEEE Trans. Wireless Commun.*, vol. 15, no. 3, pp. 2312–2327, 2016.
- [24] X. Zhou, R. Zhang, and C. K. Ho, "Wireless information and power transfer: Architecture design and rate-energy tradeoff," *IEEE Trans. Commun.*, vol. 61, no. 11, pp. 4754–4767, 2013.
- [25] G. Zhu, Y. Du, D. Gündüz, and K. Huang, "One-bit over-the-air aggregation for communication-efficient federated edge learning: Design and convergence analysis," *to appear in IEEE Trans. Wireless Commun.*, 2020.
- [26] H. Yu, S. Yang, and S. Zhu, "Parallel restarted SGD with faster convergence and less communication: Demystifying why model averaging works for deep learning," in *Proc. AAAI Conf. Artif. Intell.*, Honolulu, USA, Jan 27 - Feb 1, 2019.
- [27] D. Basu, D. Data, C. Karakus, and S. Diggavi, "Qsparse-local-SGD: Distributed SGD with quantization, sparsification and local computations," in *Proc. Adv. Neural Inf. Process. Syst. (NeurIPS)*, Vancouver, Canada, Dec 8-14, 2019.
- [28] A. Koloskova, S. Stich, and M. Jaggi, "Decentralized stochastic optimization and gossip algorithms with compressed communication," in *Proc. Int. Mach. Learn. Res. (ICLR)*, Long Beach, USA, Jun 9-15, 2019.
- [29] F. Zhou and G. Cong, "On the convergence properties of a k-step averaging stochastic gradient descent algorithm for nonconvex optimization," in *Proc. Int. Joint Conf. Artif. Intell., (IJCAI)*, Stockholm, Sweden, Jul 13-19, 2018.
- [30] F. Baccelli, B. Blaszczyszyn, and P. Muhlethaler, "An aloha protocol for multihop mobile wireless networks," *IEEE Trans. Inf. Theory*, vol. 52, no. 2, pp. 421–436, 2006.
- [31] B. McMahan, E. Moore, D. Ramage, S. Hampson, and B. A. y Arcas, "Communication-efficient learning of deep networks from decentralized data," in *Proc. Int. Conf. Artif. Intell. Statist. (AISTATS)*, Fort Lauderdale, USA, Apr 20-22, 2017.
- [32] X. Zhang, X. Zhou, M. Lin, and J. Sun, "Shufflenet: An extremely efficient convolutional neural network for mobile devices," in *Proc. IEEE/CVF Conf. Comput. Vision Pattern Recognit. (CVPR)*, Salt Lake City, USA, Jun 18-23, 2018.
- [33] C. Liu, J. Li, W. Huang, J. Rubio, E. Speight, and F. Lin, "Power-efficient time-sensitive mapping in heterogeneous systems," in *Proc. Int. Conf. Parallel Archit. Compilation Tech. (PACT)*, Minneapolis, USA, Sep 21-25, 2012.
- [34] J. Bernstein, Y.-X. Wang, K. Azizzadenesheli, and A. Anandkumar, "signSGD: Compressed optimisation for non-convex problems," in *Proc. Int. Conf. Mach. Learn.*, Stockholm, Sweden, Jul 10-15, 2018.
- [35] F. Sattler, S. Wiedemann, K. R. Müller, and W. Samek, "Robust and communication-efficient federated learning from non-i.i.d. data," *IEEE Trans. Neural Netw. Learn. Syst.*, vol. 31, no. 9, pp. 3400–3413, 2020.
- [36] Z. Allen-Zhu, "Natasha 2: Faster non-convex optimization than SGD," in *Proc. Adv. Neural Inf. Process. Syst. (NeurIPS)*, Montreal, Canada, Dec 2-8, 2018.
- [37] L. Bottou, F. E. Curtis, and J. Nocedal, "Optimization methods for large-scale machine learning," *SIAM Rev.*, vol. 60, no. 2, pp. 223–311, 2018.
- [38] J. Wu, W. Hu, H. Xiong, J. Huan, V. Braverman, and Z. Zhu, "On the noisy gradient descent that generalizes as SGD," [Online] <https://arxiv.org/pdf/1906.07405.pdf>, 2019.
- [39] F. F. Stephan, "The expected value and variance of the reciprocal and other negative powers of a positive bernoullian variate," *Ann. Math. Statist.*, vol. 16, no. 1, pp. 50–61, 1945.